Consortium for Small-Scale Modelling

Technical Report No. 18

Statistical analysis of high-resolution COSMO Ensemble forecasts in view of Data Assimilation

April 2010

DOI: 10.5676/DWD_pub/nwv/cosmo-tr_18

Deutscher Wetterdienst

MeteoSwiss

Ufficio Generale Spazio Aereo e Meteorologia

ΕΘΝΙΚΗ ΜΕΤΕΩΡΟΛΟΓΙΚΗ ΥΠΗΡΕΣΙΑ

Instytucie Meteorogii i Gospodarki Wodnej

Administratia Nationala de Meteorologie

Agenzia Regionale per la Protezione Ambientale del Piemonte

Agenzia Regionale per la Protezione Ambientale dell' Emilia-Romagna: Servizio Idro Meteo

Centro Italiano Ricerche Aerospaziali

Amt für GeoInformationswesen der Bundeswehr

www.cosmo-model.org

Editor: Massimo Milelli, ARPA Piemonte
Printed at Deutscher Wetterdienst, P.O. Box 100465, 63004 Offenbach am Main

Statistical analysis of high-resolution COSMO Ensemble forecasts in view of Data Assimilation

Daniel Leuenberger

MeteoSwiss
Krähbühlstrasse 58
8044 Zürich
Switzerland

Contents

Abstract

Data assimilation techniques based on the statistical least squares theory or the best linear unbiased estimate (BLUE), such as variational or ensemble Kalman filter methods rely on the assumption that the model first guess and the observations are bias free and its errors are normally distributed with known variances and covariances. Nonlinearities, resulting from strong dynamical instabilities can result in non-Gaussian error distributions and thus potentially cause problems in data assimilation.
In this study, error distributions of the non-hydrostatic COSMO model in a convection-permitting deterministic and ensemble configuration are investigated. Forecast departures and ensemble background anomalies of varying lead time and different variables are considered for this purpose.
The forecast departures of most of the investigated variables show a reasonable Gaussian behaviour around the median, but exhibit more larger departures (both negative and positive) than described by a normal distribution ("fat tails"). Near-surface variables tend to be closer to normality than upper-level variables. Humidity and rainfall show a rather exponential than Gaussian behaviour.
Ensemble background anomalies at short lead times can deviate significantly from normality. Especially low-level temperature has been found to have multiple modes in their distribution. At longer lead times the anomaly distributions are much closer to normality. Upper level distributions are close to Gaussian. The large deviations from normality at short lead times are largely due to the physical perturbations employed in the current COSMO ensemble system to introduce spread.
Overall, the results of this study suggest that, ensemble data assimilation systems relying on the BLUE theory may well be feasible for the use with the high-resolution COSMO model, given that appropriate (i.e. more random) physics parametrisation perturbations are applied.

1 Introduction

Ensemble Kalman filter based assimilation methods for numerical weather prediction models currently receive considerable attention in the scientific community. While first implementations for global models are already operationally employed, the development of such schemes for regional [mesh size O(10km)] and convection permitting scale [mesh size O(1km)] models is still in its infancy. The COSMO consortium (http://www.cosmo-model.org) is currently developing a new ensemble assimilation system for its convection permitting NWP model. The Local Ensemble Transform Kalman Filter (LETKF, Hunt et al., 2007) is an ensemble Kalman filter method based on the statistical least squares theory or the best linear unbiased estimate (BLUE). Assimilation methods based on this theory (e.g. variational methods, ensemble Kalman filter methods) allow an optimal combination of model and observations, given that the basic assumptions of the BLUE theory are met, namely that the model first guess and the observations are bias free and its errors are normally distributed with known variances and covariances. The violation of the Gaussian assumption has found to be of concern in non-mean-preserving deterministic square-root filters (Sakov and Oke, 2008), where the ensemble can show a tendency to develop markedly non-Gaussian error distributions (Lawson and Hansen, 2004; Leeuwenburgh et al., 2005; Mitchell and Houtekamer, 2009). In these studies, the stochastic ensemble Kalman filter with perturbed observations seemed largely immune to this problem, even in strongly nonlinear applications. On the other hand, Bonavita et al. (2010) demonstrated that the LETKF works reasonable in a regional NWP system with distributions that slightly deviate from Normality. Yang and Kalnay (2009) and Kalnay and Yang (2009) proposed ways to deal with strong non-linearities and non-Gaussianity using the LETKF in iterative ways.

In an ensemble Kalman filter approach, the optimal combination of model forecast and observations, called analysis, can formally be determined by finding the minimum of the cost function

$$J(\mathbf{x}) = \left(\mathbf{x} - \bar{\mathbf{x}}^{\mathbf{b}}\right)^T \left(\mathbf{P}^b\right)^{-1} \left(\mathbf{x} - \bar{\mathbf{x}}^{\mathbf{b}}\right) + \left[\mathbf{y_o} - H(\mathbf{x})\right]^T \mathbf{R}^{-1} \left[\mathbf{y_o} - H(\mathbf{x})\right] \tag{1}$$

$\mathbf{x}$ is the multidimensional model state vector, $\bar{\mathbf{x}}^{\mathbf{b}}$ is the ensemble mean of the model background, defined by the average of all ensemble members $\mathbf{x}^{b(i)}, i = 1..k$

$$\bar{\mathbf{x}}^{\mathbf{b}} = k^{-1} \sum_{i=1}^{k} \mathbf{x}^{b(i)} \tag{2}$$

$\mathbf{P}^b$ is the background error covariance matrix, $\mathbf{y_o}$ is the observation vector, H is the observation operator and $\mathbf{R}$ is the observation error covariance matrix. The forecast departures $\mathbf{d} = \mathbf{y_o} - H(\mathbf{x})$ measure the difference between observations and model equivalents. The ensemble background anomaly (EBA) $\mathbf{a}_i$ is defined by the difference of a particular ensemble member and the ensemble mean $\mathbf{a}_i = \mathbf{x}^{b(i)} - \bar{\mathbf{x}}^{\mathbf{b}}$.

Even though the LETKF is by construction a mean-preserving ensemble square-root filter and thus should be less prone to problems with non-Gaussianity it is worth looking at how well the convection permitting COSMO model meets the assumption of the BLUE theory, namely how well the forecast departure statistics and the ensemble background anomalies can be approximated by a Gaussian distribution. The questions to be answered are

- What form take the distributions of forecast departures and EBA from a short-range high-resolution (ensemble) COSMO forecast ?
- How does the distribution changes with forecast lead time ?

- Are there differences in the distribution between summer and winter ?

The results are expected to give a hint if the LETKF is feasible to be used with the convection permitting COSMO model.

2 Data and Evaluation Method

2.1 Data

2.1.1 Forecast Departures

The forecast departure statistics considered in this study are based on operational DWD convection permitting COSMO-DE (mesh size of 2.8 km, without parametrized deep convection, covering Germany and surroundings) and regional COSMO-EU (mesh size of 7 km, with deep convection parametrization, covering whole Europe) forecasts from two periods:

- Winter: 12/2007 - 02/2008 (91 days, 364 forecasts)
- Summer: 06/2008 - 08/2008 (92 days, 368 forecasts)

Since we are interested in short-range forecasts we consider departures for forecast lead times from +3h to +6h. In order to see how the statistics change with evolving forecast time, we compare them with departures for leadtimes from +9 to +12h. Forecast departures are calculated for all conventional observations that are routinely assimilated in the COSMO model at DWD, namely

- SYNOP (p_s,T,u/v,RH, and pp)
- Radiosondes (T,u/v and RH at 940, 850, 500 and 300 hPa)
- Aircraft data (T and u/v at 940, 850, 500 and 300 hPa)
- Wind profiler (u/v at 940, 850, 500 and 300 hPa)

All observations from the above list are actively assimilated, except surface precipitation (pp) from SYNOP stations, which is only used for the calculation of the departures.

For ease of comparison of COSMO-DE and COSMO-EU, only departures from observations inside the COSMO-DE domain are taken into account.

2.1.2 Ensemble Background Anomalies

The ensemble background anomalies are calculated from forecasts of the pre-operational high resolution German COSMO-DE EPS, running in a similar configuration as the COSMO-DE deterministic forecast. The 20 ensemble forecast members are initialized at 00 UTC from a regional EPS (COSMO-SREPS) driven by different global models and using different physical parametrization settings and are integrated out to 24 hours. The configuration of the boundary conditions and of the physical parametrisations are summarized in Table 1.

- Ensemble forecast from a summer period (8.8.2007 - 16.8.2007) are considered.
- Forecast lead times of +3h and +24h are compared
- The following variables are looked at
  - T and u at the terrain-following model levels at approximately 10 m, and 5500 m above surface.
  - pp at the surface

Ensemble members	Driving global model	
01-05	ECMWF	
06-10	GME	
11-15	NCEP	
16-20	UKMO	
Ensemble members	Physical parameter perturbation	Default value
01, 06, 11, 16	entrscv=0.002	entrscv=0.0003
02, 07, 12, 17	clc_diag=0.75	clc_diag=0.5
03, 08, 13, 18	rlam_heat=50	rlam_heat=1
04, 09, 14, 19	rlam_heat=0.1	rlam_heat=1
05, 10, 15, 20	tur_len=150	tur_len=500

Table 1: Configuration of the COSMO-DE EPS in terms of boundary conditions and physical parametrisation tuning values.

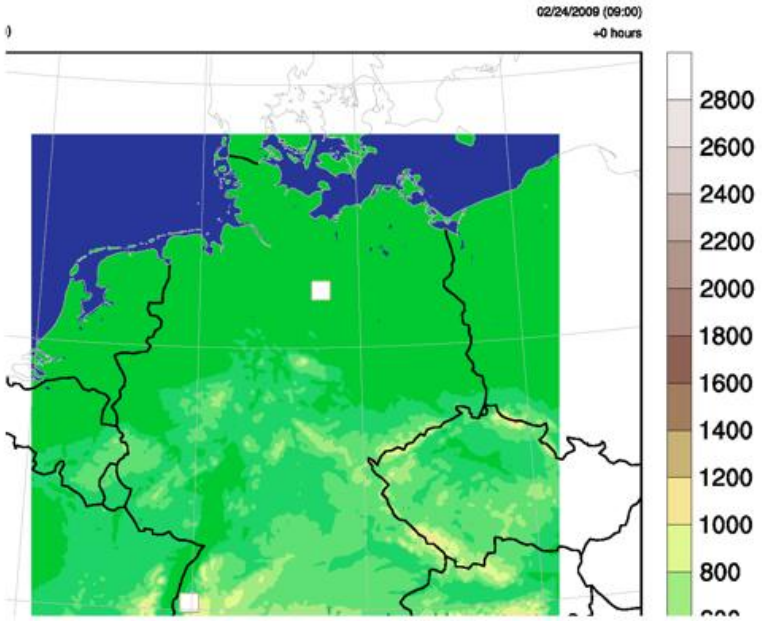

Figure 1: Computational domain of COSMO-DE and COSMO-DE EPS. The coloured domain depicts the plotting domain for the stamp maps in Section 4 and the two white squares marks the two verification domains South Germany and North Germany used for the calculation of the ensemble anomaly statistics.

2.2 Evaluation Method

In order to judge, how well the forecast departure and EBA distributions are approximated by the Gaussian distribution, we compare them, both qualitatively and more quantitatively with Gaussian pdf's fitted to the data. The forecast departure d_l of a single observation is

$$d_l = y_{o,l} - H(\mathbf{x})_l \tag{3}$$

where y_0 denote the observation and $H(\mathbf{x})_l$ the corresponding model equivalent obtained by the application of the observation operator H to the model state $\mathbf{x}$. $l = 1..N_l$ is the index specifying a particular observation from all N_l observations.

For the ensemble background anomalies we consider all k ensemble members and compute the distribution from all anomalies $a_{(i,j)}$, $i = 1..k$, $j = 1..N_j$, where N_j is the number of gridpoints of a 2d model field in a specified verification domain and at a certain terrain-following level.

The probability distribution $p(x)$ over a set of indices i (e.g. all temperature observations from radiosondes at $850 \pm 10hPa$ within a leadtime range of +3h to +6h using COSMO-DE forecasts in the summer period) is considered (near-)Gaussian if it approximates the Gaussian distribution

$$\tilde{p}(x) = N(\bar{x}, \sigma) = \frac{1}{\sqrt{2\pi}\sigma} e^{-\left(\frac{x-\bar{x}}{\sigma}\right)^2} \tag{4}$$

The mean $\bar{x}$ and the standard deviation σ of the distributions are calculated by

$$\bar{x} = \frac{1}{N}\sum_{i=1}^{N} x_i \tag{5}$$

$$\sigma = \sqrt{\frac{1}{N}\sum_{i=1}^{N}\left(x_i - \bar{x}\right)^2} \tag{6}$$

where N is the number of data in the considered set.

In the case of the forecast departures, $x = d, i = l$ and $N = N_l$. In the case of the ensemble background anomalies, $x = \mathbf{a}$ and $N = N_j \cdot k$. The qualitative evaluation of the Gaussianity of $p(x)$ is done graphically by plotting the pdf and its Gaussian approximation $\tilde{p}(x)$ calculated from (4) using (5) and (6). Figure 2 (upper panel) shows an example for a forecast departure distribution: the bold line represents the pdf $p(d)$ and the thin line its approximation $\tilde{p}(d)$. Note that in the semilogarithmic representation the normal pdf takes a parabolic form.

It is useful to not only estimate if the Gaussian approximation is fulfilled, but to estimate how well it is approximated. To this end we define the term "normrange" by the range of probabilities over which the Gaussian approximation is reasonable. A perfect Gaussian fit has a normrange of 100%. To calculate the normrange, a normal probability plot is drawn of $p(x)$. In this graph, the cumulative distribution function of $p(x)$ is transformed in a way that a Gaussian distribution represents a straight line. Any deviation from this line suggests non-Gaussianity. The reference Gaussian distribution, against $p(x)$ is compared, is obtained from the 25% and the 75% quantile of $p(x)$. It appears as the dash-dotted straight lines on the normal probability plots. The normrange is then calculated as the range, where $p(x)$ is close to the line. "Close" is defined such that $p(x)$ does not differ from the straight line by more than a threshold, defined by the difference of the 25% and the 75% quantile divided by 12 (subjective choice). Figure 2 (lower panel) shows an example of a normal probability plot. The crosses borders the normrange, i.e. the region where $p(x)$ can be reasonably approximated by the normal distribution.

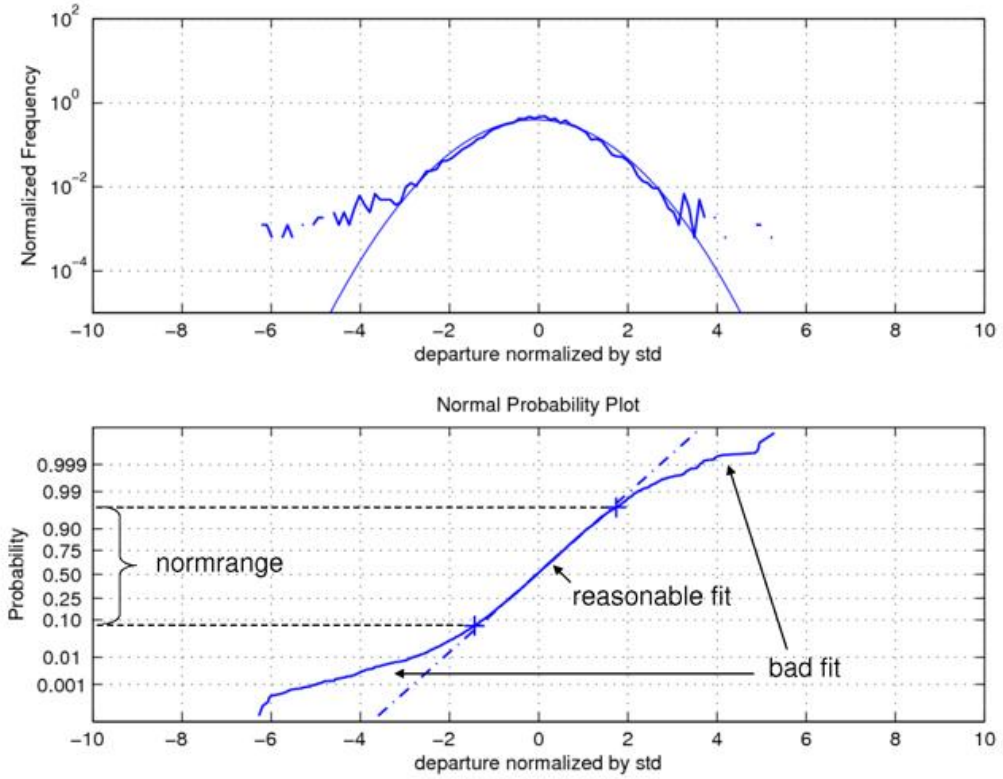

Figure 2: Example of the evaluation method used in this study. Upper panel: semilogarithmic representation of the departure distribution $p(d)$ (bold line) and its reference normal distribution $\tilde{p}(d)$ (thin line). Lower panel: normal probability plot and definition of normrange (see also text).

3 Forecast Departure Statistics

In this section we present COSMO-DE forecast departure distributions from all observations in the model domain mentioned in Section 2.1.

3.1 Near surface

3.1.1 Surface Pressure

Figure 3 shows the results for surface pressure. The distribution is near-Gaussian around the median and within approximatively ± 3 standard deviations, which corresponds to roughly ± 2.7 hPa, irrespective of the forecast lead time. At the end (tails) of the distributions, the departure distribution deviates from normality, i.e. there are more large deviations than what would be described by a Gaussian distribution. The distribution is slightly asymmetric at the tails, i.e. there are more large positive departures than large negative departures, meaning that the model more often largely underestimates pressure than largely overestimates it.

The negative pressure bias (i.e. in the mean, the model overestimates the pressure) increases by 17% in summer (26% in winter) with lead time (upper panels). The normranges amount to roughly 94% in summer and 87% in winter (lower panels) and do not change significantly during the first 12h of the forecast.

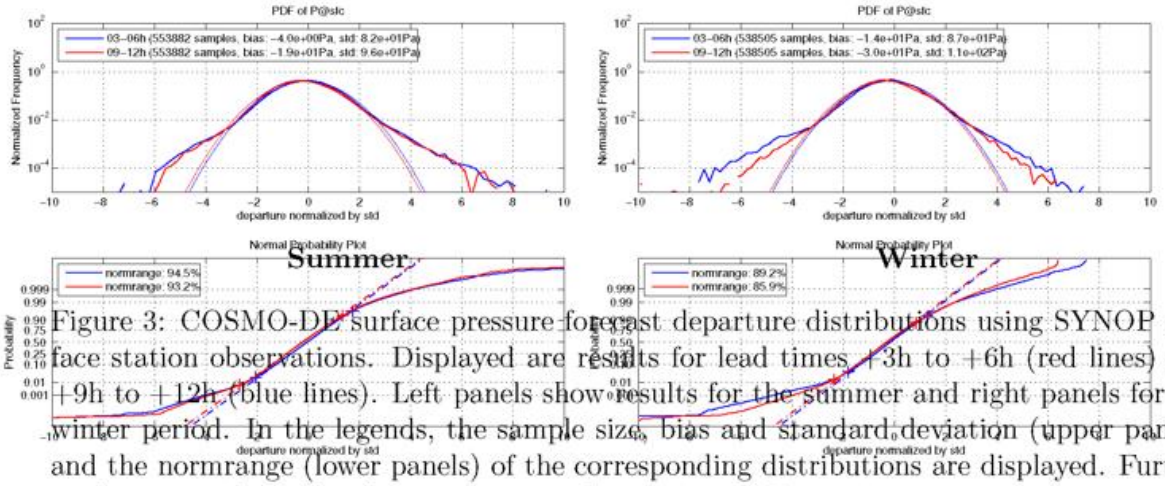

Figure 3: COSMO-DE surface pressure forecast departure distributions using SYNOP surface station observations. Displayed are results for lead times +3h to +6h (red lines) and +9h to +12h (blue lines). Left panels show results for the summer and right panels for the winter period. In the legends, the sample size, bias and standard deviation (upper panels) and the normrange (lower panels) of the corresponding distributions are displayed. Further explanations about the plots are given in Section 2 and Figure 2.

3.1.2 2m Temperature

The 2m temperature distributions differ from the surface pressure distributions in that they are less good approximated by a normal distribution (Figure 4). This is particularly obvious in winter (right upper panel), but to a less degree also in summer (left upper panel). The

lognormal curves have a more linear than parabolic shape, suggesting a more exponential than Gaussian nature. This behaviour is reflected in normranges of approx. 83% in summer and 75% in winter. The bias are below one degree and the standard deviations around 1.8 degrees. Both bias and standard deviation are nearly leadtime independent up to 12h.

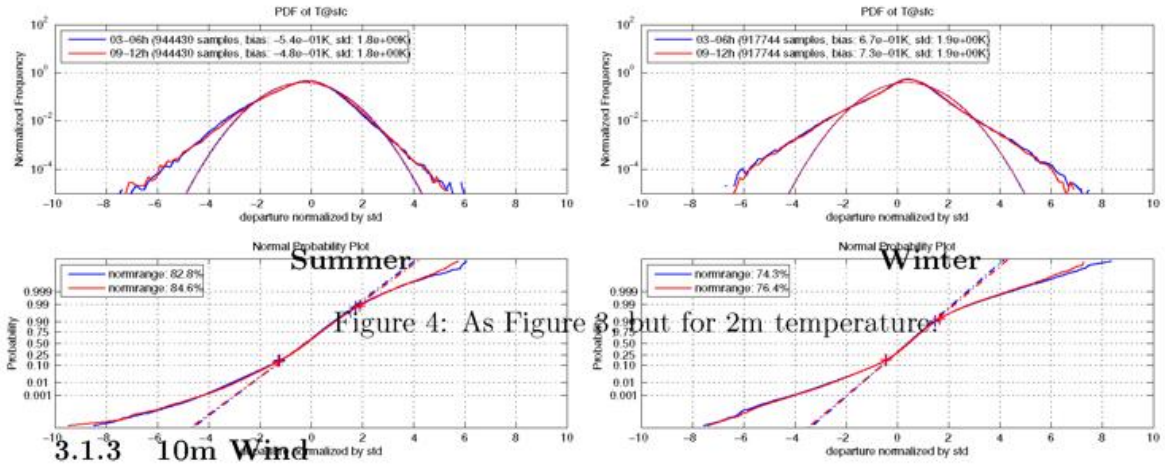

Figure 4: As Figure 3, but for 2m temperature.

3.1.3 10m Wind

The distributions of 10m wind are better Gaussian approximated than those of 2m temperature (Fig. 5). Normranges are about 89% in summer and 84% in winter.

The bias is around -0.1 m/s and the standard deviation around 1.8 m/s and nearly independent from lead time and season. Zonal and meridional components behave almost identically, therefore only the zonal wind speed is shown.

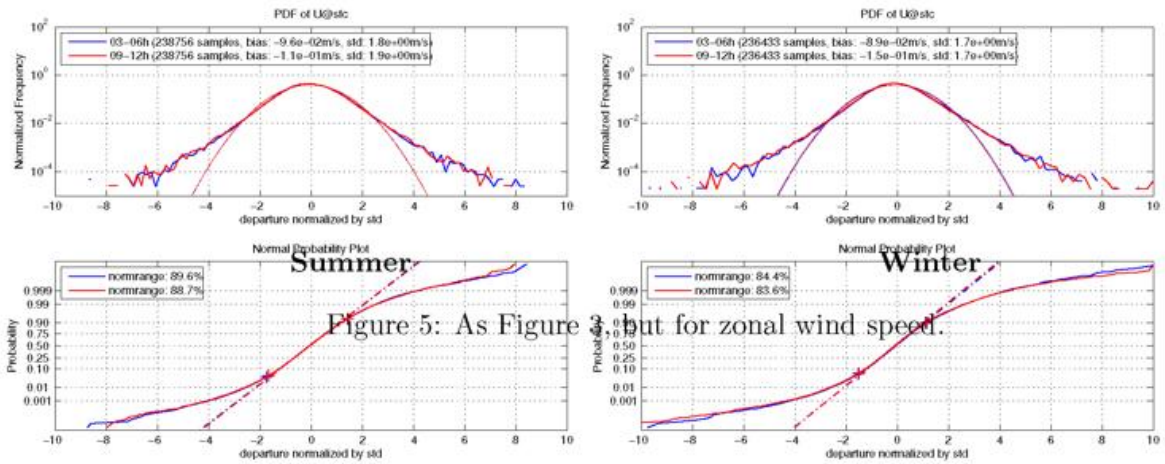

Figure 5: As Figure 3, but for zonal wind speed.

3.1.4 2m Humidity

The 2m relative humidity forecast departure distribution (Fig. 6) differs substantially between summer and winter. In summer the distribution is very close to normal, even the negative "fat tail" is absent, resulting in a high normrange of 88%. In winter the distribution is more exponential than Gaussian and thus the normrange does not exceed 79%. The distributions are nearly independent on lead time.

Also the bias is dependent on season and amounts 5.4% (-1%) in summer (winter). The standard deviation is in both seasons 11%.

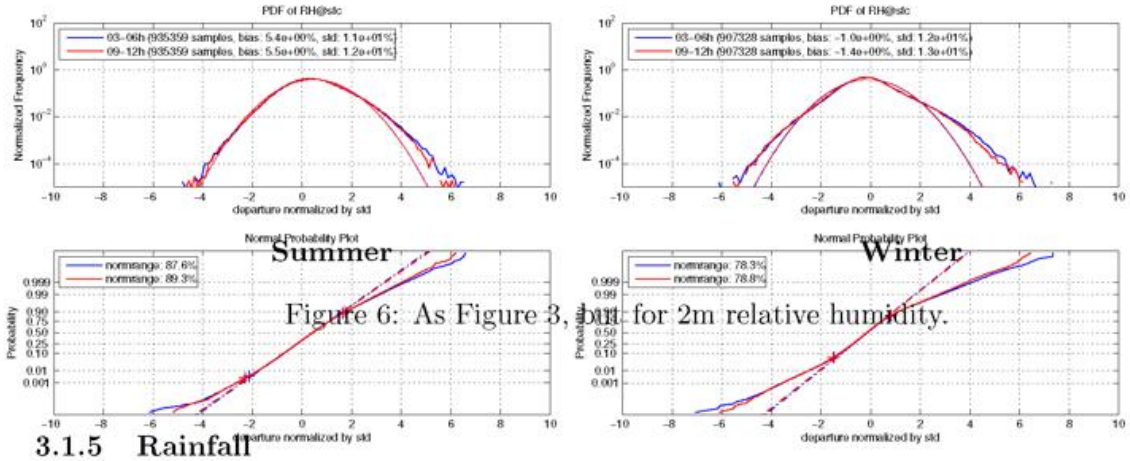

Summer **Winter**

Figure 6: As Figure 3, but for 2m relative humidity.

3.1.5 Rainfall

Surface rainfall as observed by SYNOP stations is not actively assimilated in the model, but merely used to compute forecast departures. The distribution turns out to be far away from Gaussian both, in summer and winter (Figure 7). The normrange calculation is not reliably applicable for this type of distribution and is therefore omitted.

Summer **Winter**

Figure 7: As Figure 3, but for rainfall observed by SYNOP.

Forecast departures from radar rainfall have been computed using model output from the Swiss COSMO-2 (mesh size of 2.2 km, without parametrized deep convection) which runs in a similar configuration as the COSMO-DE model and from radar derived surface rainfall from the Swiss Radar Network (SRN). The model data is taken from 13 12UTC forecasts (same lead times as before) during the period from 1.6.2008 to 13.6.2008. A domain of 70x40 km with a very good radar visibility in the Swiss plateau has been chosen, in order to

obtain high quality observations. The departures are calculated gridpoint by gridpoint from hourly sums after a 3x3 gridbox filter application. Radar rainfall is assimilated in the high resolution COSMO-DE and the Swiss COSMO-2 using the latent heat nudging scheme.

As for SYNOP rainfall, the departures using radar rainfall (Figure 8) can not be approximated with a Gaussian distribution. A distinct peak at zero departure suggests the occurrence of many situations where rain is neither observed nor forecast. Beyond standard deviations of 1 (-1) the distribution shows an exponential rather than a Gaussian behaviour. Moreover the distribution is asymmetric and exhibits more large positive departures (i.e. underestimation by the model).

Figure 8: As Figure 7, but for Swiss summer rainfall derived from radar data.

3.2 Upper atmosphere

Upper air measurements are classified according to the pressure level, on which they are observed. Main pressure levels of 940, 850, 500 and 300 hPa are considered in this study. For the sake of increasing the sample size, observations within a pressure layer with thickness of 20 hPa centered around the main pressure level are also taken into account. Forecast departures have been calculated from radiosonde, aircraft and windprofiler observations. The distributions are of similar structure between corresponding observations, though they slightly differ in bias and standard deviation. Therefore, only the observations with the largest sample size are shown here (aircraft data for temperature and wind and radiosonde data for humidity), the rest of the results are shown in Section 5.

3.2.1 Temperature

Upper air temperature forecast departures can generally be well approximated by Gaussian distributions (Figures 9 - 12 and 38 - 41). Only in the winterly boundary layer (at 940 hPa and 850 hPa), deviations between 0 and -2 standard deviations are apparent. Normranges reach values of 86%-96% in summer and 79%-90% in winter. Values in the boundary layer are generally lower than in the middle and upper atmosphere.

Biases are well below 0.2 K and standard deviations below 1.5 K. Departures are larger in winter and in the boundary layer than in summer and in the mid/upper atmosphere.

3.2.2 Wind

Wind departures are found to be also very nearly Gaussian (Figures 13 - 16 and 42 - 61). Normranges are between 79% and 88%, generally higher in summer than in winter, but there is no clear dependence on height.

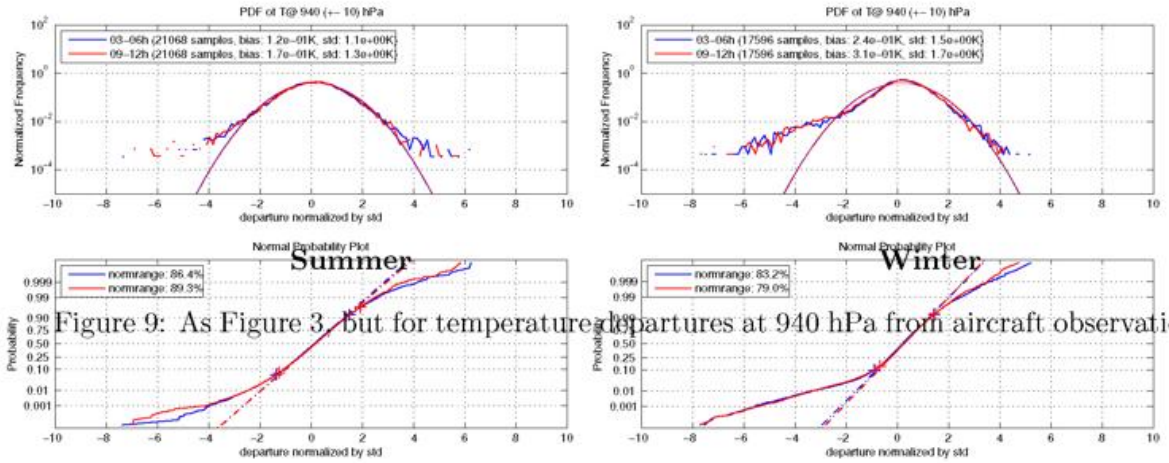

Figure 9: As Figure 3, but for temperature departures at 940 hPa from aircraft observations.

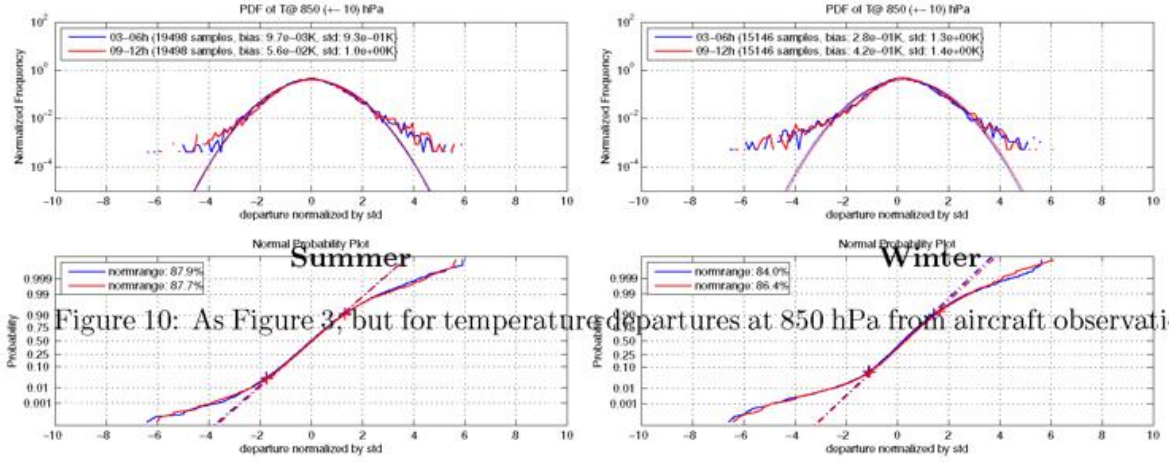

Figure 10: As Figure 3, but for temperature departures at 850 hPa from aircraft observations.

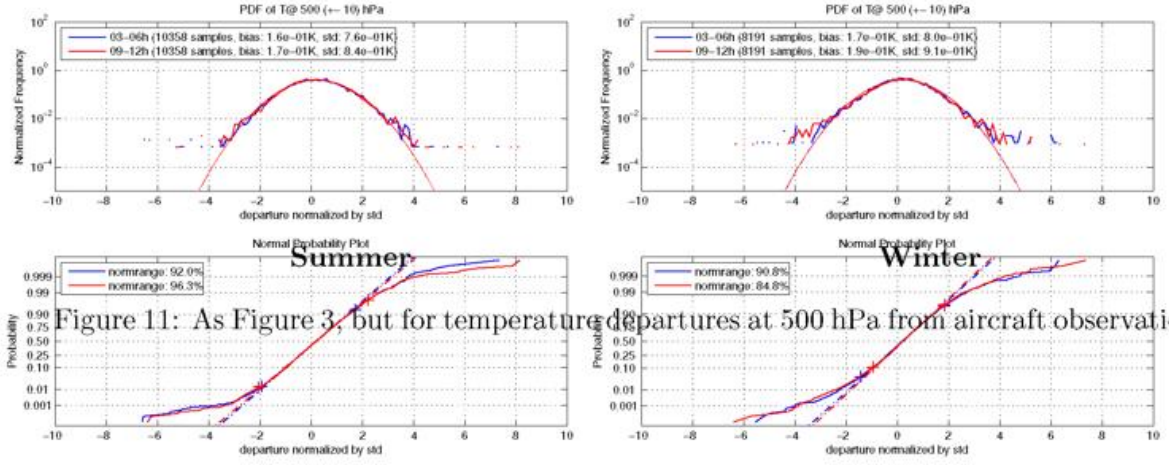

Figure 11: As Figure 3, but for temperature departures at 500 hPa from aircraft observations.

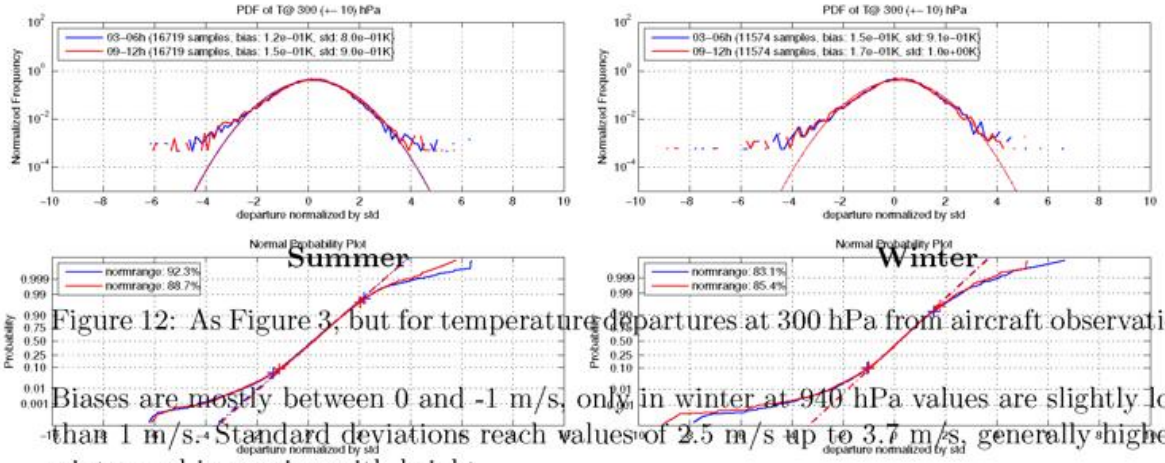

Figure 12: As Figure 3, but for temperature departures at 300 hPa from aircraft observations.

Biases are mostly between 0 and -1 m/s, only in winter at 940 hPa values are slightly lower than 1 m/s. Standard deviations reach values of 2.5 m/s up to 3.7 m/s, generally higher in winter and increasing with height.

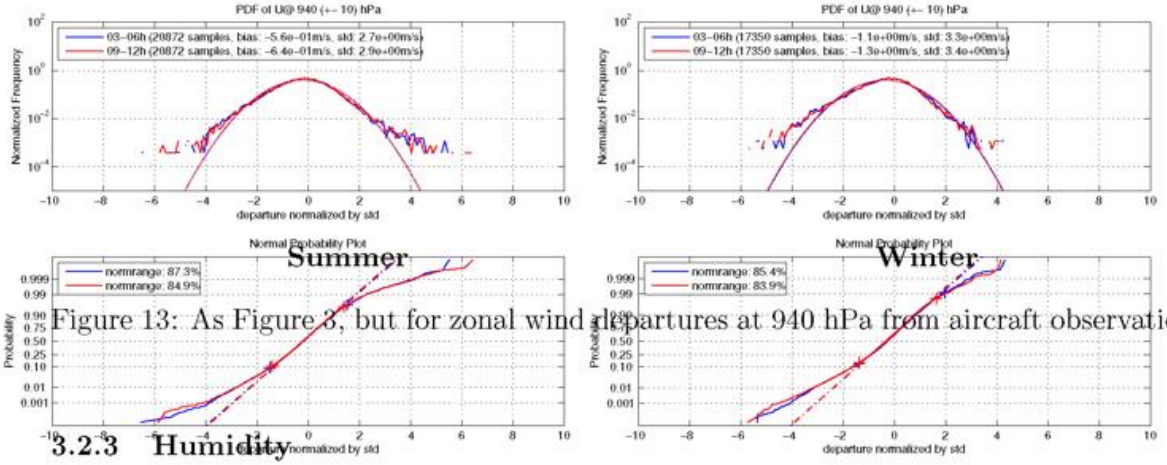

Figure 13: As Figure 3, but for zonal wind departures at 940 hPa from aircraft observations.

3.2.3 Humidity

Forecast departures of relative humidity can not be well approximated by a normal distribution (Figures 17 - 20). Especially in winter a distinct peak in the pdf is visible for zero departures in the boundary layer (940 hPa and 850 hPa, Figures 17 and 18). This peak origins from many winterly stratus situations, where both model and observations are saturated, resulting in zero departures (not shown). This peak is not apparent in summer and in the upper atmosphere. Winter distributions generally show a rather exponential, than Gaussian shape, resulting in generally low normranges, where summer distributions are more Gaussian.

Biases increase with height from less than 2% (940 hPa) to roughly -9% (300 hPa) in summer and 3% (940 hPa) to roughly -7% (300 hPa) in winter. Standard deviations are less height-

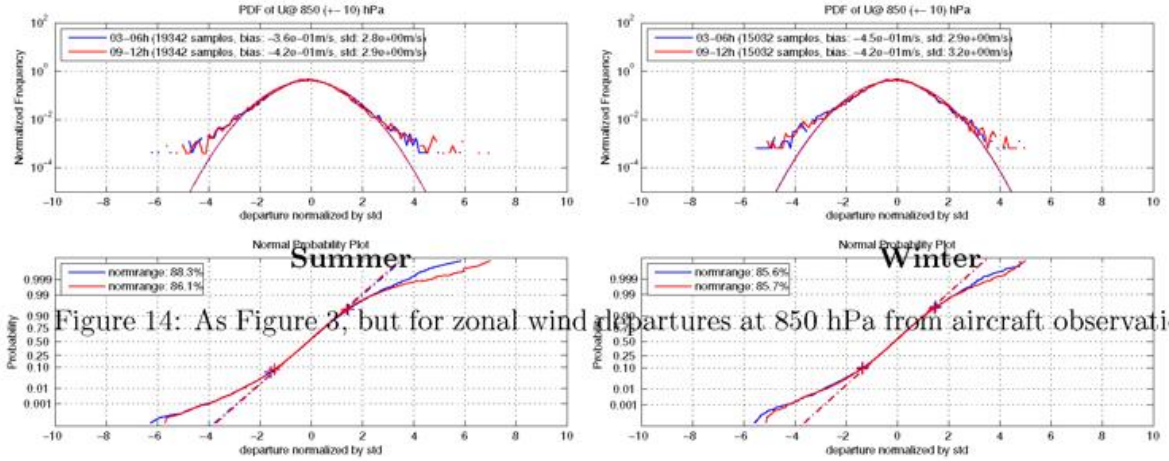

Figure 14: As Figure 3, but for zonal wind departures at 850 hPa from aircraft observations.

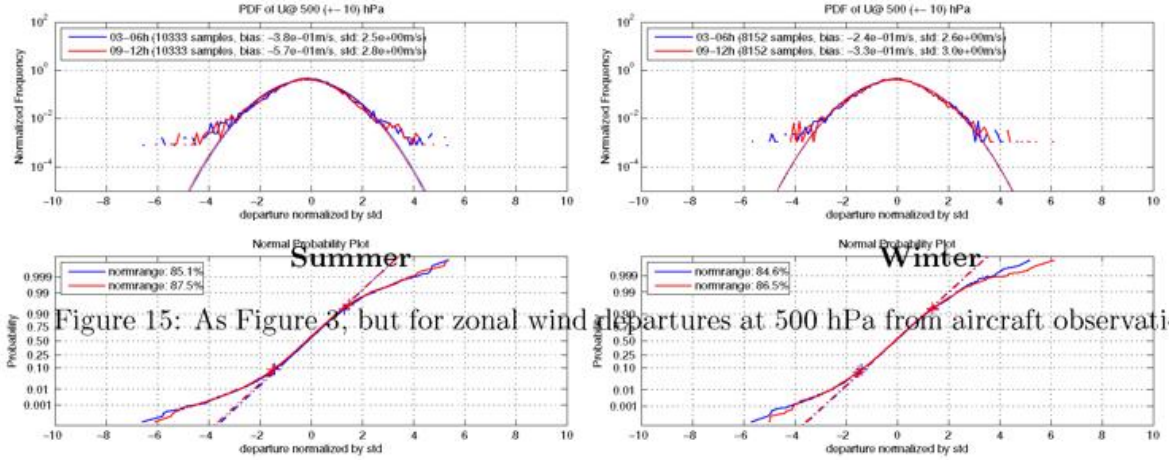

Figure 15: As Figure 3, but for zonal wind departures at 500 hPa from aircraft observations.

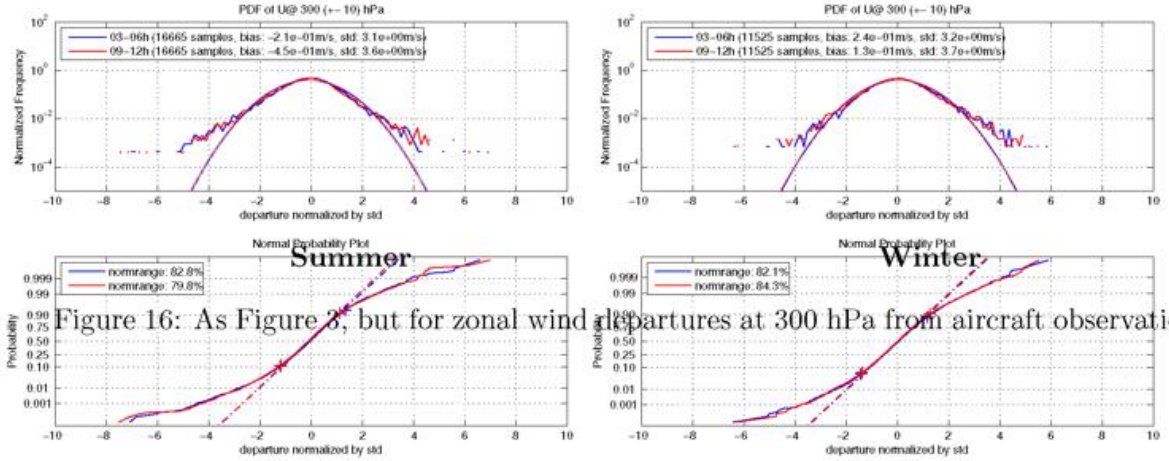

Figure 16: As Figure 3, but for zonal wind departures at 300 hPa from aircraft observations.

dependent and reach values of 15%-20% both in summer and winter. The errors only slightly increase in the first 12h.

Summer **Winter**

Figure 17: As Figure 3, but for relative humidity departures at 940 hPa from radiosonde observations.

Summer **Winter**

Figure 18: As Figure 3, but for relative humidity departures at 850 hPa from radiosonde observations.

Summer **Winter**

Figure 19: As Figure 3, but for relative humidity departures at 500 hPa from radiosonde observations.

Summer **Winter**

Figure 20: As Figure 3, but for relative humidity departures at 300 hPa from radiosonde observations.

3.3 Sensitivity studies

3.3.1 Dependency on Humidity variable

The forecast departure distributions of humidity and rainfall turned out to be the least Gaussian of all model variables. In this section other forms of humidity are investigated, namely specific humidity, the logarithm of specific humidity, a normalized relative humidity (Holm et al., 2002) and the logarithm of rainfall.

Humidity In this section, alternative humidity representations to the relative humidity are looked at. Holm et al. (2002) looked at different humidity variables for the assimilation in the ECMWF IFS model and proposed a normalized relative humidity (NRH) with appealing properties for the assimilation:

- the bias $\bar{d}$ is effectively eliminated, a prerequisite for a successful assimilation
- Forecast departure distributions are near-Gaussian over the whole range of relative humidity values, especially near saturation and in very dry situations, which is not the case for relative humidity departures

The normalized relative humidity departure (d_{NRH}) is calculated following Holm et al. (2002)

$$d_{NRH} = \frac{d_{RH}}{\sigma\left(RH_m + d_{RH}/2\right)}, \tag{7}$$

where the numerator is the standard relative humidity departure (d_{RH}) and the denominator is the standard deviation of the sum of model value (RH_m) and relative humidity departure divided by two.

Figure 21 shows results of COSMO-DE forecast departures using different representations of humidity observations from radiosondes at 850 hPa. Displayed are results for lead times +3h to +6h (red lines) and +9h to +12h (blue lines). Left panels show results for the summer and right panels for the winter period. Obviously, departures of specific humidity (first row) and its logarithm (second row) are less Gaussian than relative humidity (third row), particularly in summer (left panels). Departures of NRH (lowest row) show a similar Gaussian approximation but both bias and standard deviation are reduced by more than an order of magnitude as compared to those using relative humidity.

In order to see how the distributions behave in near saturated or very dry situations, forecast departures have been calculated conditional to the modelled relative humidity. Due to small sample sizes in summer, only the results of the winter period are shown. The upper panels

of Figure 22 show departures of relative humidity for situations where model values exceed 85% (blue lines) and very dry situations (relative humidity below 15%, red lines). Both distributions show a rather exponential than a Gaussian behaviour. Moreover, both, bias and standard deviation are clearly dependent on the modelled relative humidity. In the near saturated situations the model overestimates humidity by roughly 5% (std of 13%) , whereas in dry situations the model underestimates humidity by roughly 2% (std of 1%). Note that the peak at zero departure only appears in the near saturated situations.

When using NRH as variable both biases and standard deviations are reduced by an order of magnitude (right panel of Figure 22). Moreover, the distributions of both wet and dry situations appear to be near-Gaussian.

These results confirm the findings of Holm et al. (2002) and suggest that the normalized relative humidity should have superior properties for the assimilation than the relative humidity.

Summer **Winter**

Figure 21: COSMO-DE forecast departure distributions using different representations of humidity observations from radiosondes at 850 hPa. Displayed are results for lead times +3h to +6h (red lines) and +9h to +12h (blue lines). Left panels show results for the summer and right panels for the winter period. First row: specific humidity (q_v), second row: $\log(q_v)$, third row: relative humidity (same as Figure 18) and fourth row: normalized relative humidity.

Figure 22: COSMO-DE winterly forecast departure distributions of relative humidity (left panels) and normalized relative humidity (right panel) from radiosondes at 850 hPa and forecast leadtimes from +3h to +6h. Blue lines: departures for model (normalized) relative humidity above 85% (blue lines) and departures for model (normalized) relative humidity below 15% (red lines).

Rainfall Since rainfall amounts are nearly logarithmically distributed it is obvious to look at departures of the logarithm of rainfall. Figure 23 shows the resulting distributions for rainfall (upper panels, same as Figure 7) and the logarithm of rainfall (lower panels). The forecast departures of the logarithm of rainfall are clearly much more Gaussian than those of rainfall.

The same holds true for the departures using radar-derived rainfall (Figure 24). Since the logarithm of zero is not defined, only departures with non-zero observations and model forecasts are considered. Note that in situations where only a part of the domain shows rainfall in either the observations or the model forecasts, this can reduce the sample size of the departures by orders of magnitude. Also here the distribution using the logarithm of rainfall is much more Gaussian than that using rainfall.

Summer **Winter**

Figure 23: COSMO-DE rainfall forecast departure distributions using SYNOP surface station observations. Displayed are results for lead times +3h to +6h (red lines) and +9h to +12h (blue lines). Left panels show results for the summer and right panels for the winter period. Upper panels show distributions using rainfall (same as Figure 7) and lower panels using the logarithm of rainfall.

Figure 24: Same as Figure 23 but for COSMO-2 rainfall forecast departure distributions from radar observations. Only those departures are considered where both observations and forecasts are non-zero.

3.3.2 Dependency on Model Resolution

After having investigated the forecast departures of COSMO-DE model, we are interested in how the results differ from those of the regional model COSMO-EU with a model mesh width of 7 km. The largest difference between COSMO-DE and COSMO-EU, beside their resolution, is that in COSMO-EU deep convection is parametrized, where in COSMO-DE only the shallow convection is parametrized, but deep convetion is simulated explicitly. As a result of the better resolved topography in COSMO-DE, we expect the departures to differ mostly in the boundary layer. Therefore we compare the results of the forecast departures exemplarily on the 850 hPa pressure level.

When comparing the results of COSMO-DE and COSMO-EU it gets rapidly clear that the differences in the distributions are minor in all variables and independent on season (Figures 25 - 27). Normranges do not differ by more than 3%, whereas biases and standard deviations can vary considerably depending on model parameter. The same holds true for the other observation types and differences between the two models are even smaller in the upper atmosphere (not shown).

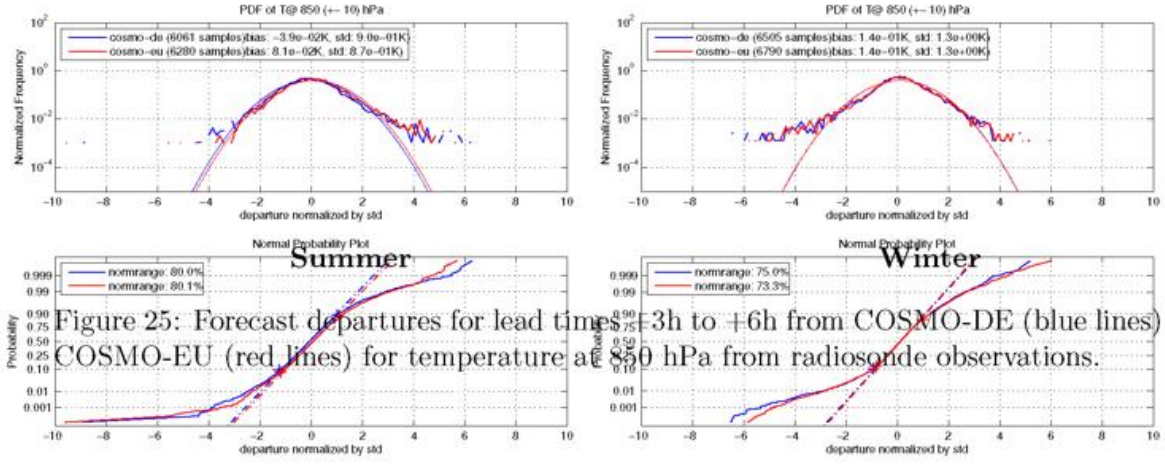

Figure 25: Forecast departures for lead times +3h to +6h from COSMO-DE (blue lines) and COSMO-EU (red lines) for temperature at 850 hPa from radiosonde observations.

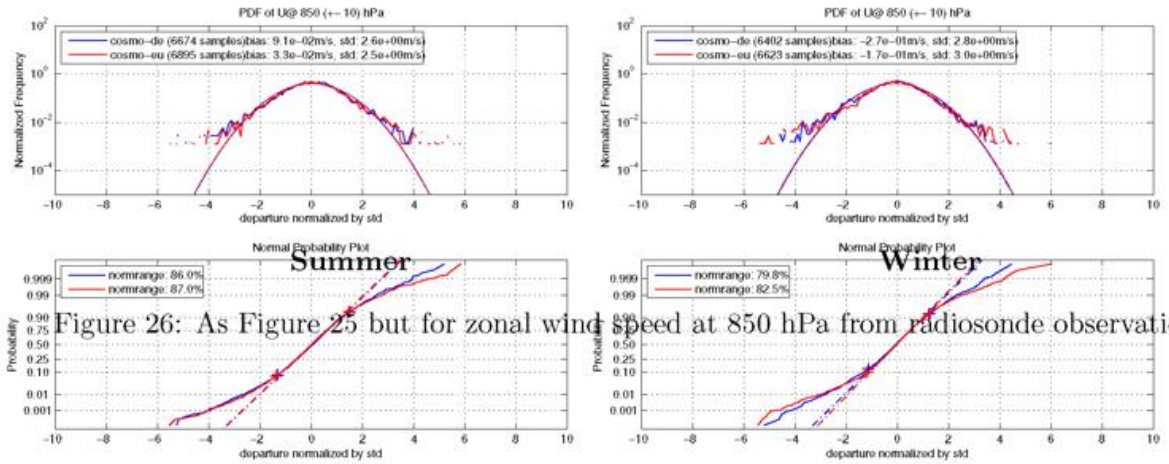

Figure 26: As Figure 25 but for zonal wind speed at 850 hPa from radiosonde observations.

Summer **Winter**

Figure 27: As Figure 25 but for relative humidity at 850 hPa from radiosonde observations.

3.3.3 Dependency on Weather Regime

All results presented so far were compiled using the whole summer (winter) period. In a sensitivity study, we stratified time according to the weather situation, i.e. we looked at the forecast departure distributions where only rainy days have been considered. We defined a rainy day as a day where a large part of the COSMO-DE domain was affected by precipitation. For this end daily accumulations from gridded raingauges have been used and a subjective separation has been made.

The resulting distributions were found to be slightly less Gaussian than those using all days for the statistics (not shown).

4 Ensemble Anomaly Statistics

In this section distributions of the ensemble background anomalies from COSMO-DE ensemble forecasts are presented. All distributions are calculated from gridpoint values of temperature and zonal wind speed at 10 m and 5400 m above surface and averaged spatially over 10x10 gridpoints of two verification domains (North and South Germany, see Figure 1) and temporally over the 9 days from 8 to 16 August 2007. Lead times of +3h and +24h are compared.

4.1 Near surface

4.1.1 Temperature

Figure 28 shows the ensemble background anomaly distribution of temperature at the lowest model level ($\approx$ 10m above surface) of the South Germany (left panel) and North Germany (right panel) verification domain. The +3h lead time distributions (blue lines) clearly show a significant deviation from normality (normrange well below 80%) for both domains. Beside the maximum around zero anomaly there is a second maximum around +2 (South Germany) and +3 (North Germany) standard deviations. On the other hand, the +24h lead time distributions (red lines) are much closer to normality (normrange above 90%) for both domains.

A closer look at the background anomalies of each ensemble member valid at 15 August 2007 03UTC (16 August 2007 00UTC) in Figure 29 (Figure 30) reveals the reason for the different distributions at +3h (+24h). At +3h (Figure 29) most members have small temperature anomalies due to the common analysis of all members. The anomalies are largely caused by the different physical parametrisations. Members 4, 9, 14, and 19 have much larger temperature anomalies than all other members. These members use a physical parametrisation tuning parameter rlam_heat = 0.1 instead of 1.0. This parameter influences the sensible heat fluxes from the surface and thus has an immediate impact on the near-surface temperature. At +24h the influence of the different boundary conditions of the driving global models on the anomalies has increased considerably (Figure 30). The amplitude of the anomalies are much larger and show more variation. The members 4, 9, 14 and 19 still show a clearly different anomaly distribution but the differences are smaller than at +3h. A similar behaviour can be found at the other days, leading to the systematic deviation from normality for the low level temperature at early lead times.

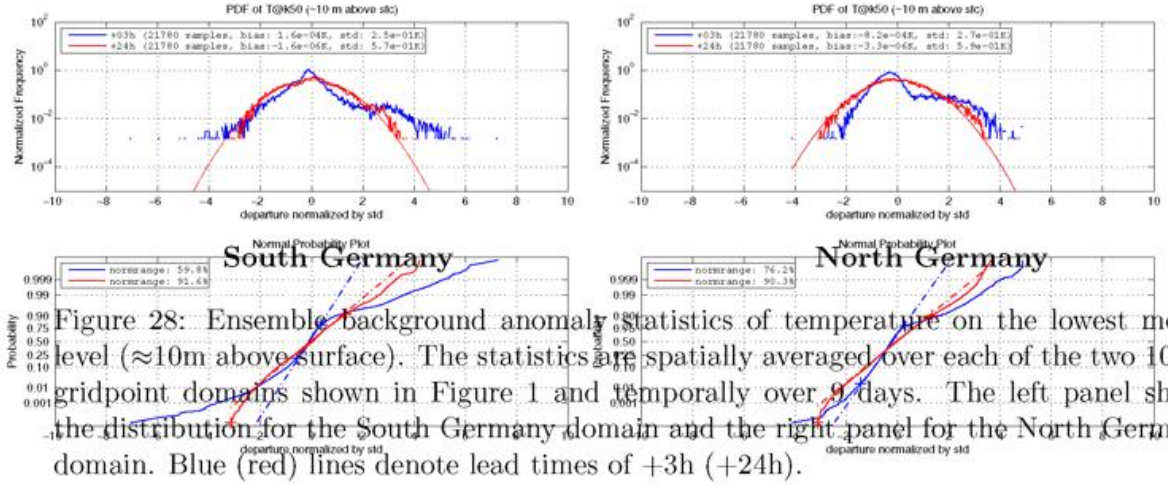

Figure 28: Ensemble background anomaly statistics of temperature on the lowest model level (≈10m above surface). The statistics are spatially averaged over each of the two 10x10 gridpoint domains shown in Figure 1 and temporally over 9 days. The left panel shows the distribution for the South Germany domain and the right panel for the North Germany domain. Blue (red) lines denote lead times of +3h (+24h).

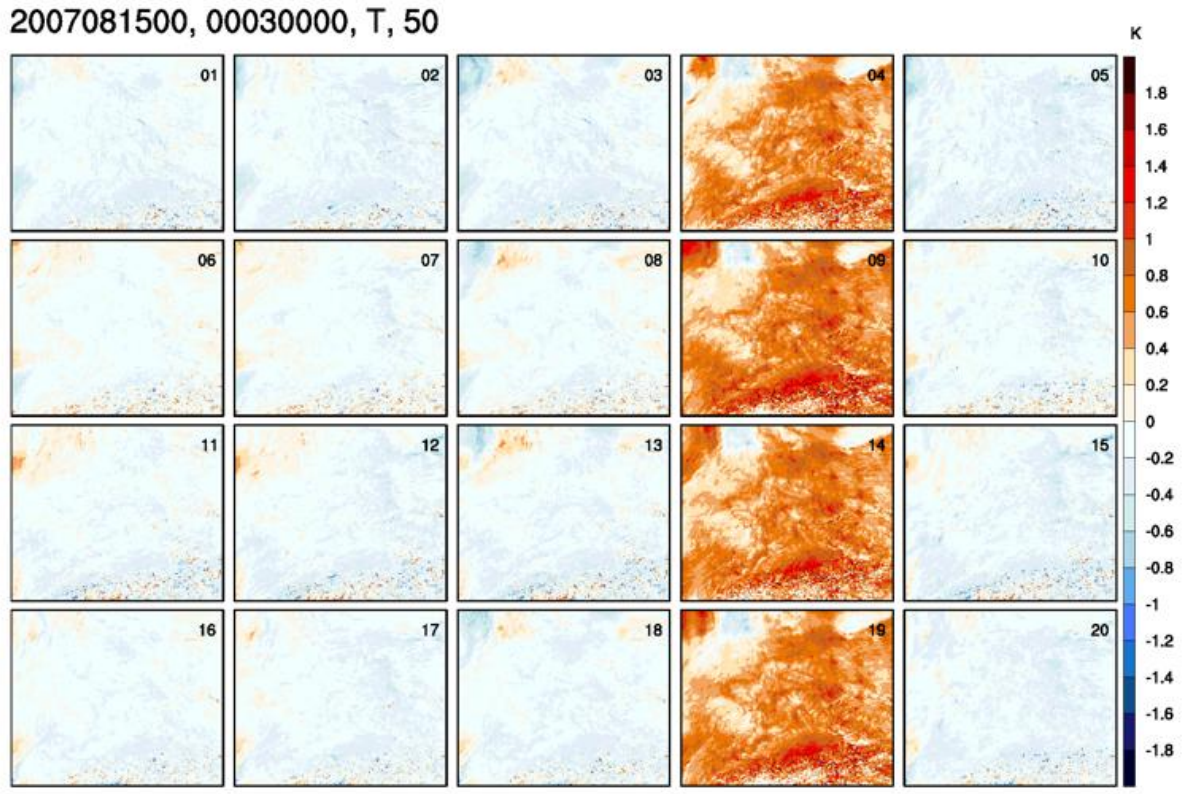

Figure 29: Stamp map of ensemble background anomalies of temperature at the lowest model level (≈10m above surface) valid at 15 August 2007 03UTC (i.e. at +3h). The domain corresponds to the coloured domain in Figure 1.

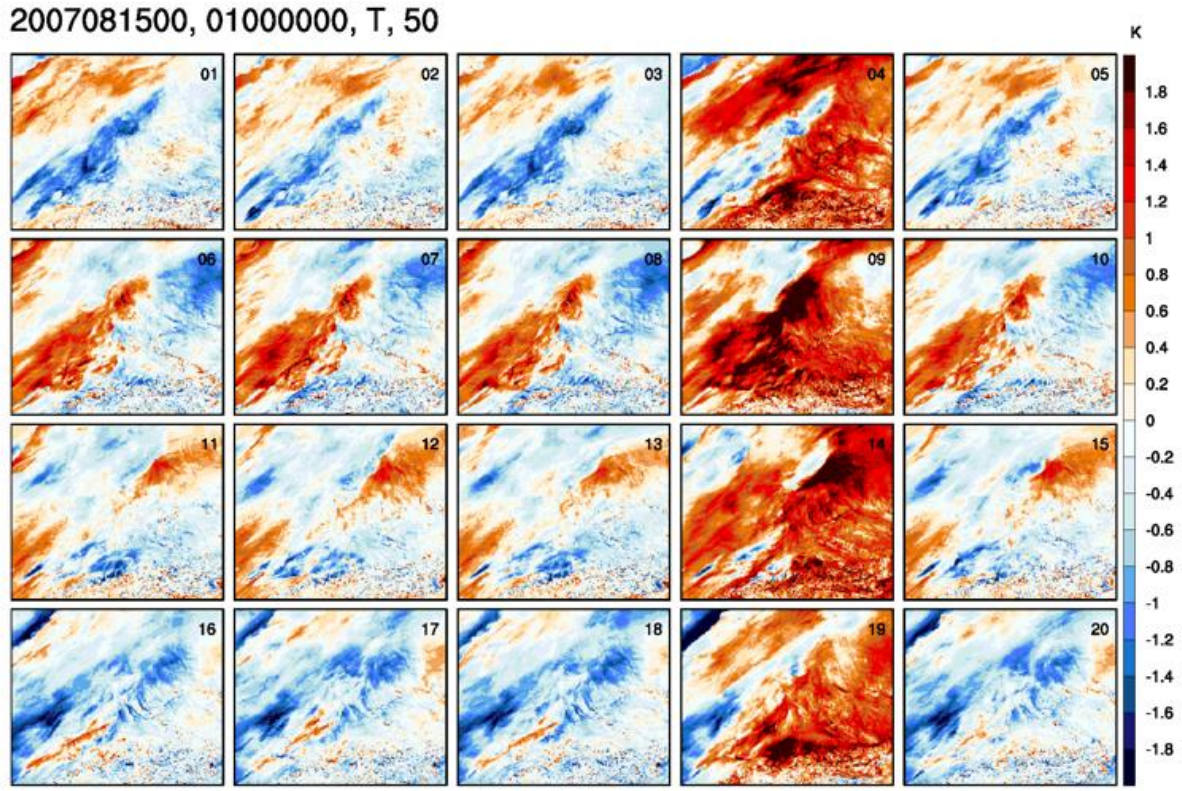

Figure 30: As Figure 29 but valid at 16 August 2007 00UTC (i.e. at +24h).

4.1.2 Wind

Figure 31 shows the distribution of zonal wind speed U at the lowest model level. The distributions at +3h and +24h are much more similar than for temperature in both domains. However, in the South Germany region, where topography is complex, the distributions show more deviations from normality than in the North Germany domain, which is essentially flat. The stamp maps in Figures 32 and 33 confirm that the anomalies are more evenly distributed in the two verification domains and all physical parametrisation settings show similar results in the wind speed.

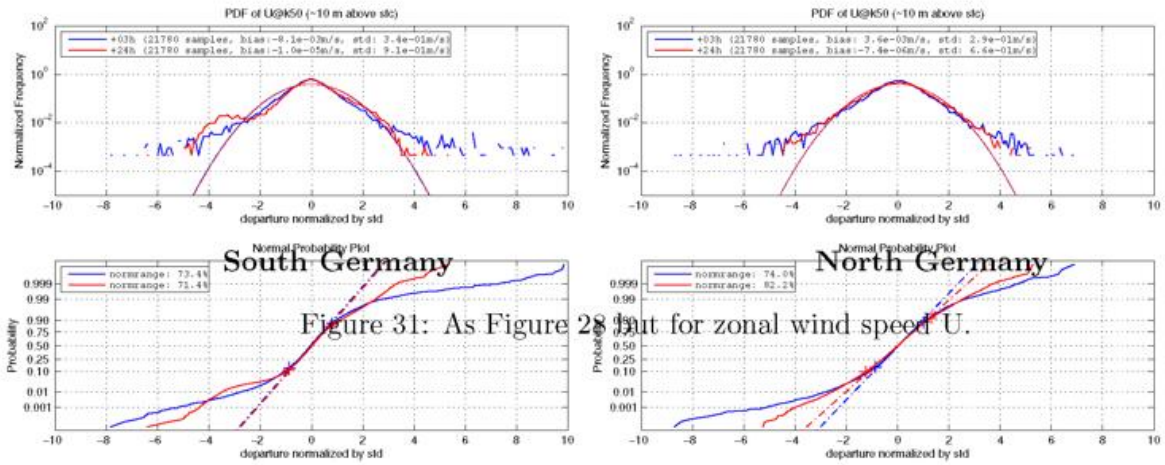

Figure 31: As Figure 28 but for zonal wind speed U.

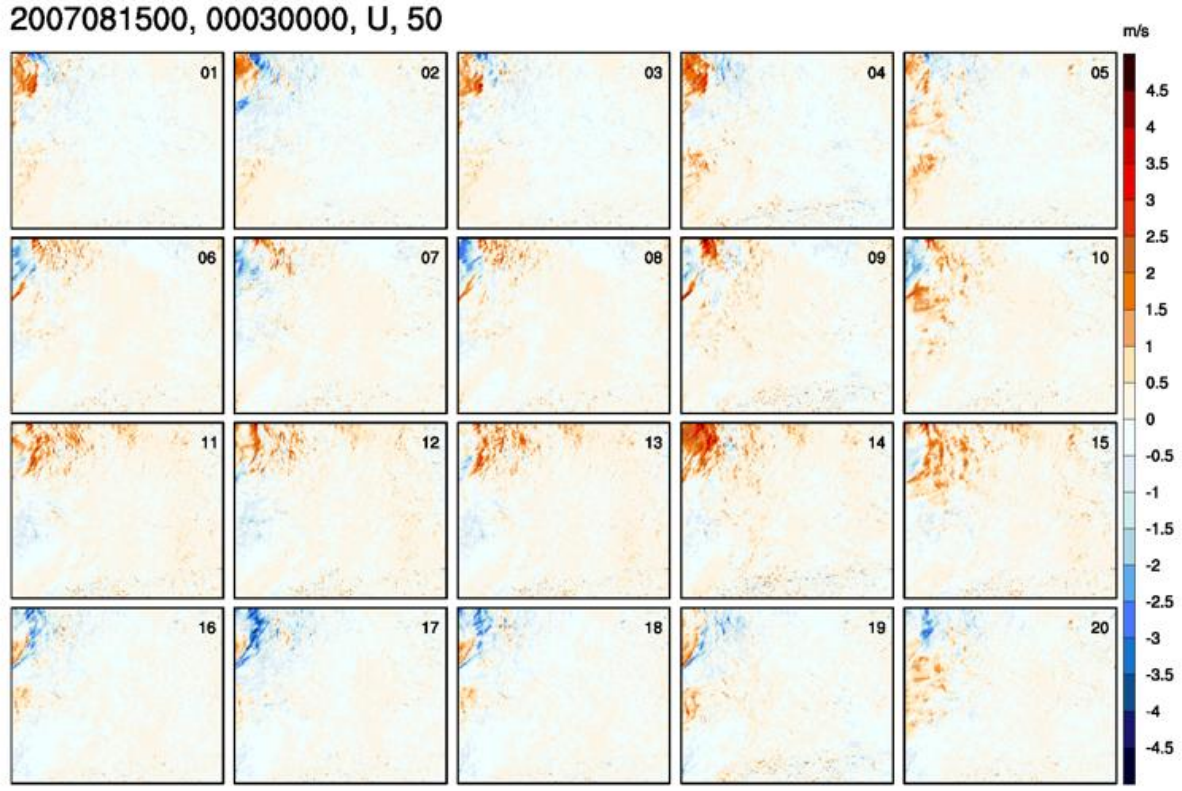

Figure 32: Stamp map of ensemble background anomalies of zonal wind speed valid at 15 August 2007 03UTC (i.e. at +3h). The domain corresponds to the coloured domain in Figure 1.

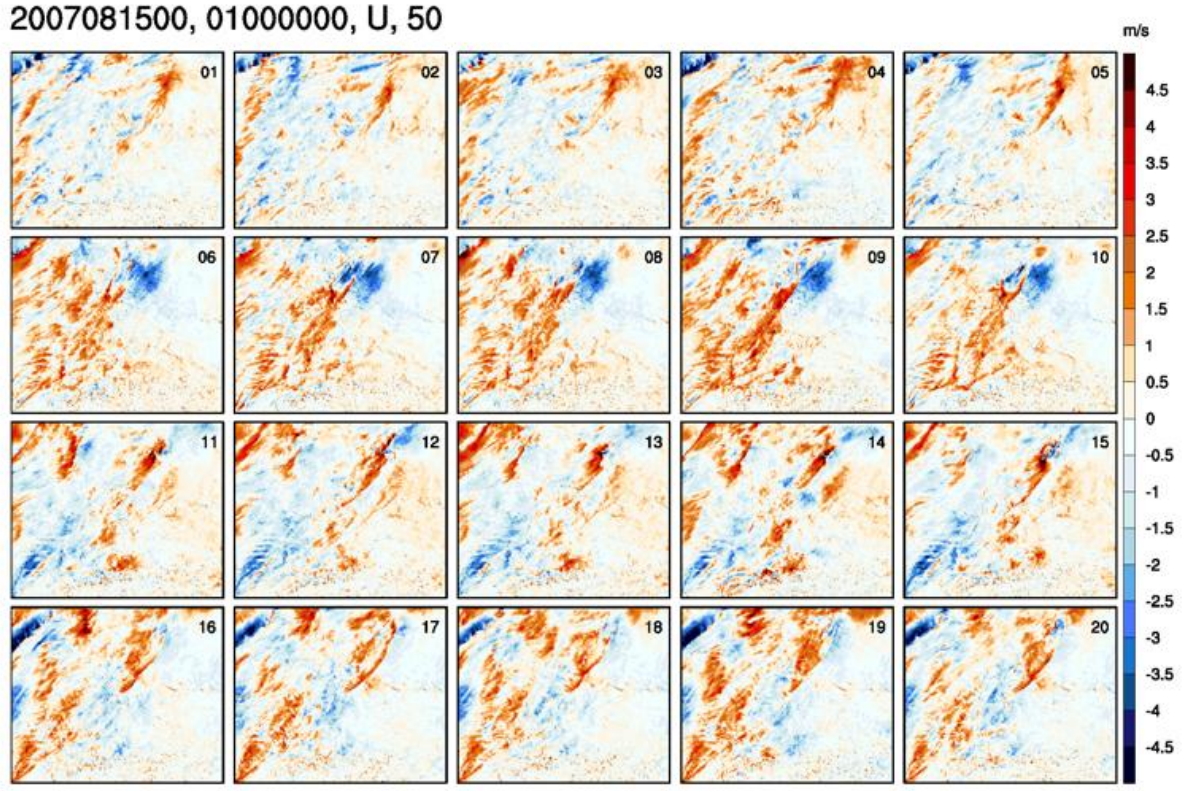

Figure 33: As Figure 29 but valid at 16 August 2007 0UTC (i.e. at +24h).

4.1.3 Precipitation

Figure 34 shows the distributions of hourly precipitation sums at lead times +2-3h and +23-24h. The distributions are clearly completely non-Gaussian at both lead times and verification domains. The stamp map in Figure 35 at +3h lead time valid at 15. August 2007 03UTC shows the reason for this. Most parts of the domain is precipitation-free and therefore anomalies are zero. In the sparse precipitation areas the anomalies take on large values, leading to a non-Gaussian distribution.

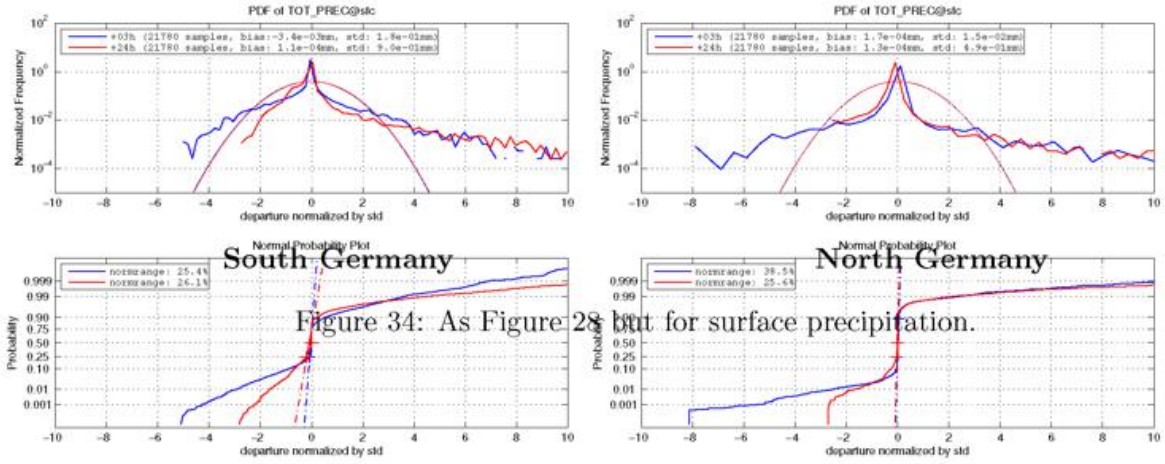

Figure 34: As Figure 28 but for surface precipitation.

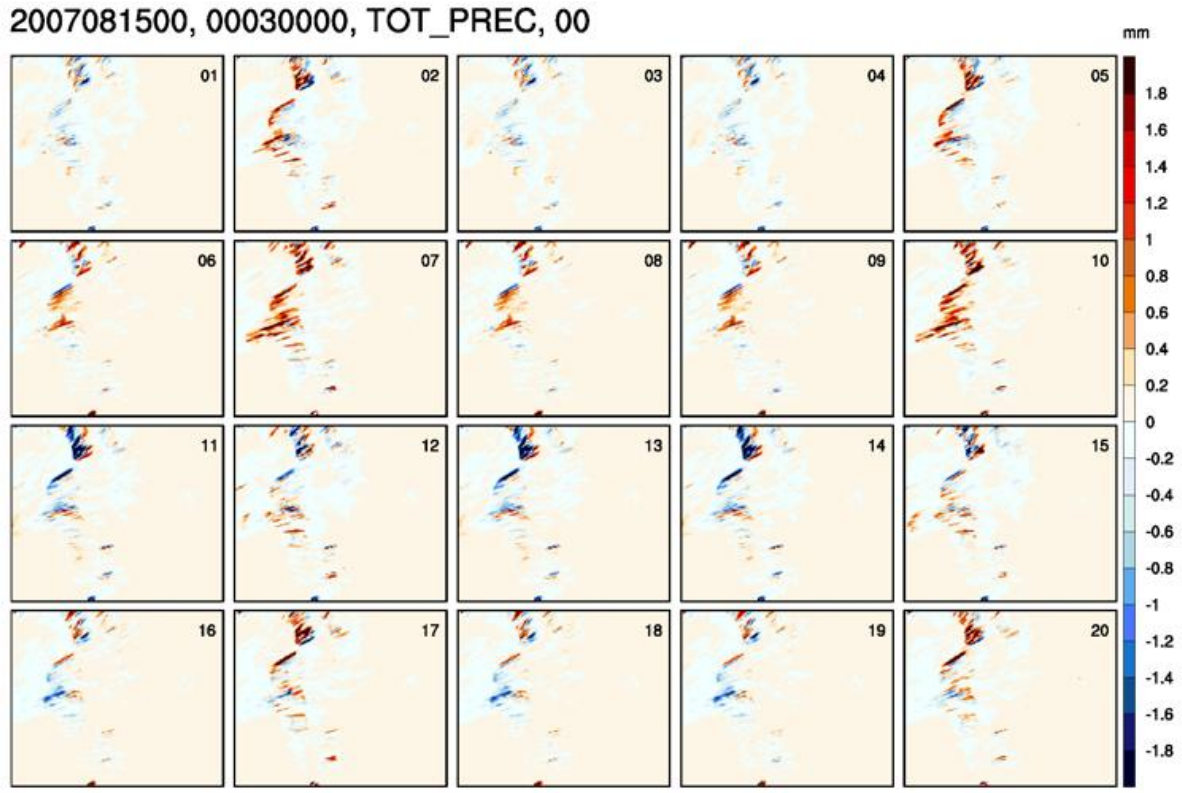

Figure 35: Stamp map of ensemble background anomalies of surface precipitation valid at 15 August 2007 03UTC (i.e. at +3h). The domain corresponds to the coloured domain in Figure 1.

4.2 Upper atmosphere

4.2.1 Temperature

Figure 36 shows the anomaly distributions for temperature on model level 24 ($\approx$ 5400 m above surface). The distributions are close to normality, both at +3h and +24 and in both verification domains. Obviously the physical parametrisation parameter affects the upper level temperature in a systematic way, as was the case in the low-level temperature.

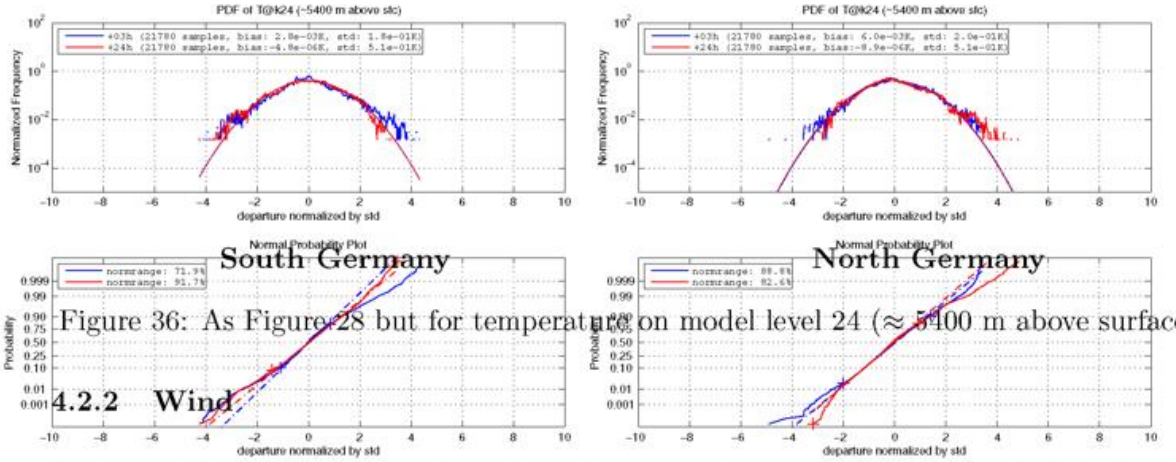

Figure 36: As Figure 28 but for temperature on model level 24 (≈ 5400 m above surface).

4.2.2 Wind

Figure 37 shows the anomaly distributions for zonal wind speed on model level 24 (≈ 5400 m above surface). The distributions are close to normality, both at +3h and +24. The distributions in the South Germany domain exhibits a slight deviation from normality, probably due to the more complex terrain which influences mid- and upper-level winds in a more systematic way than flat terrain.

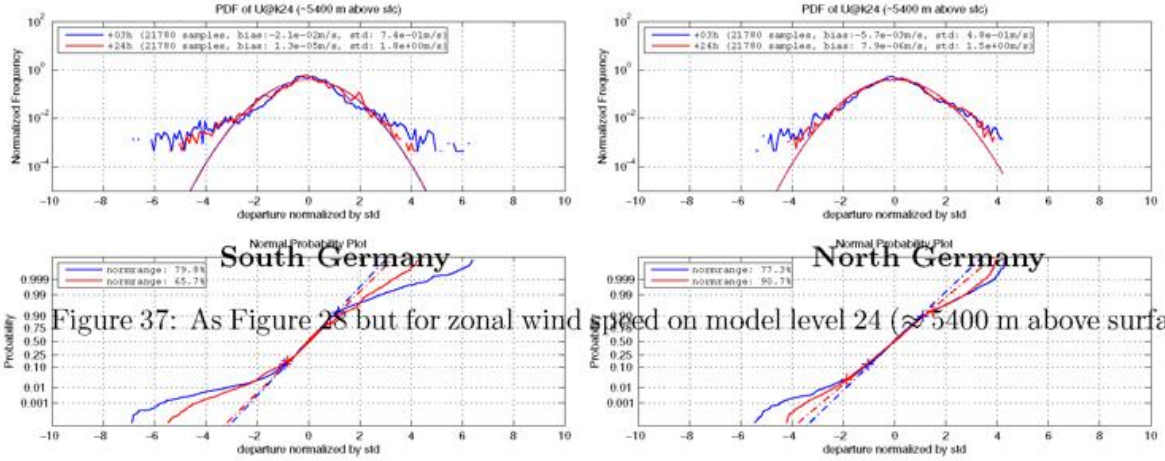

Figure 37: As Figure 28 but for zonal wind speed on model level 24 (≈ 5400 m above surface).

5 Further Results

In this section we list further results from forecast departure distributions of the COSMO-DE, which are not shown in Section 3.

5.1 Temperature from radiosondes

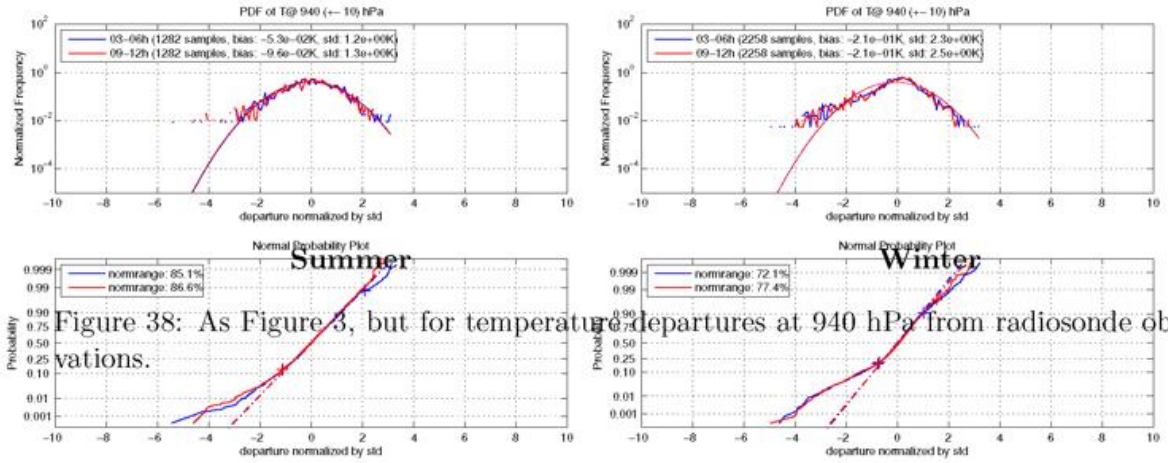

Figure 38: As Figure 3, but for temperature departures at 940 hPa from radiosonde observations.

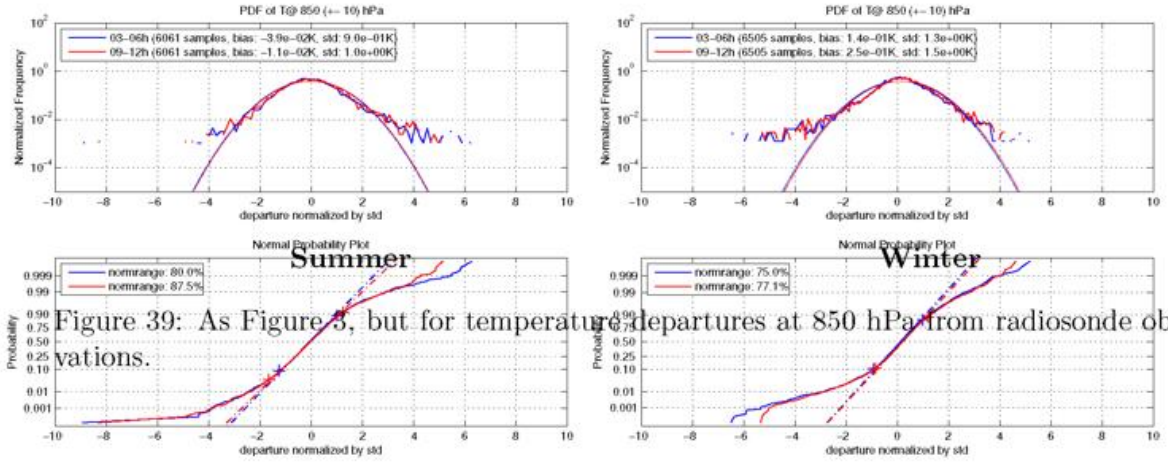

Figure 39: As Figure 3, but for temperature departures at 850 hPa from radiosonde observations.

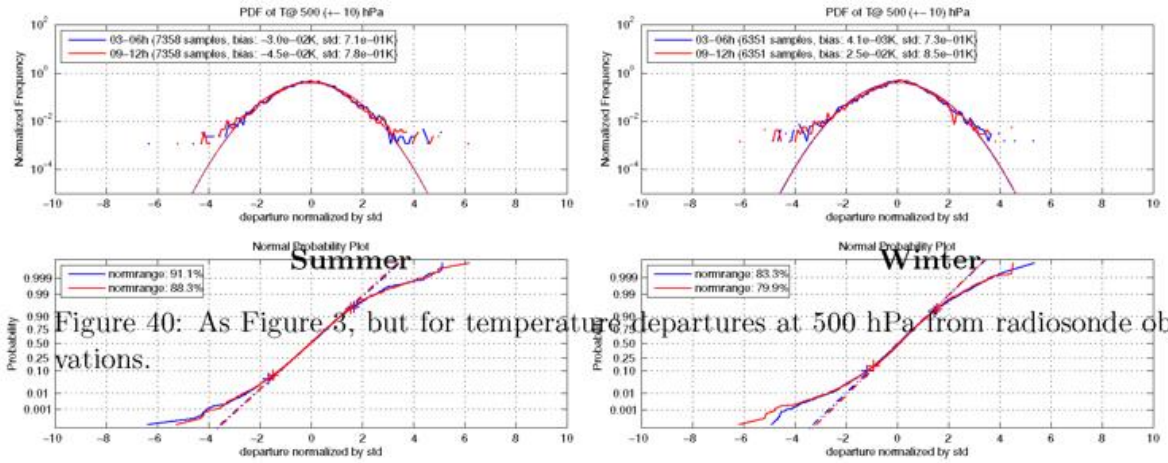

Figure 40: As Figure 3, but for temperature departures at 500 hPa from radiosonde observations.

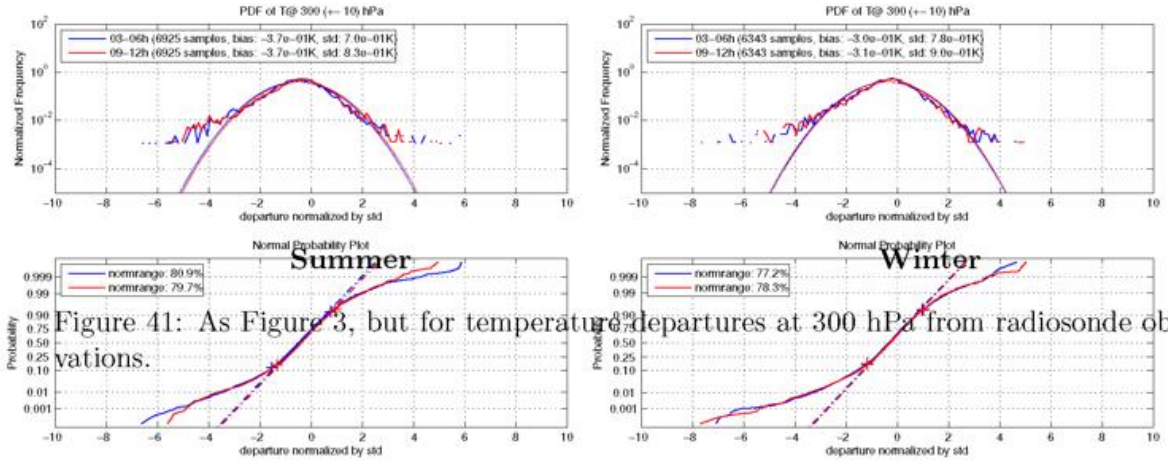

Figure 41: As Figure 3, but for temperature departures at 300 hPa from radiosonde observations.

5.2 Zonal wind from radiosondes and windprofiler

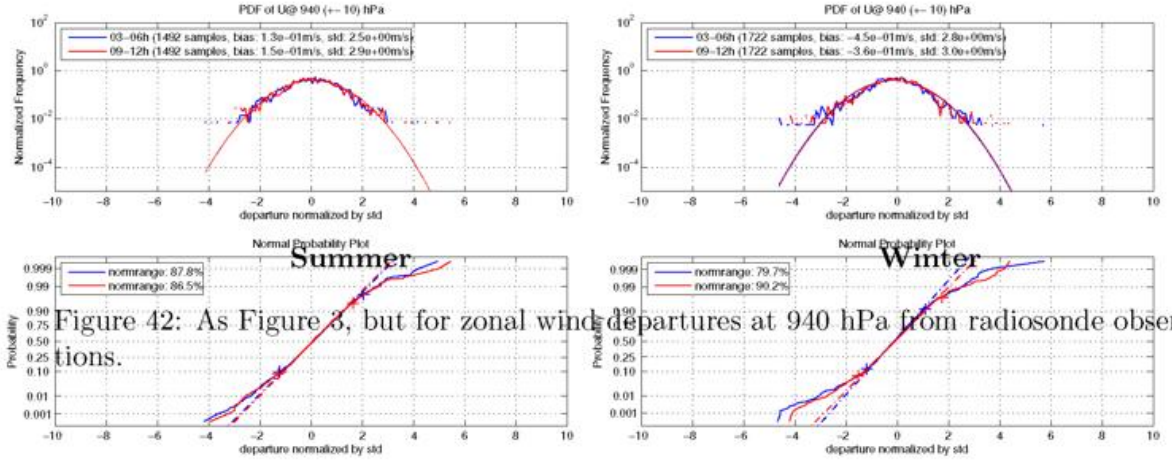

Figure 42: As Figure 3, but for zonal wind departures at 940 hPa from radiosonde observations.

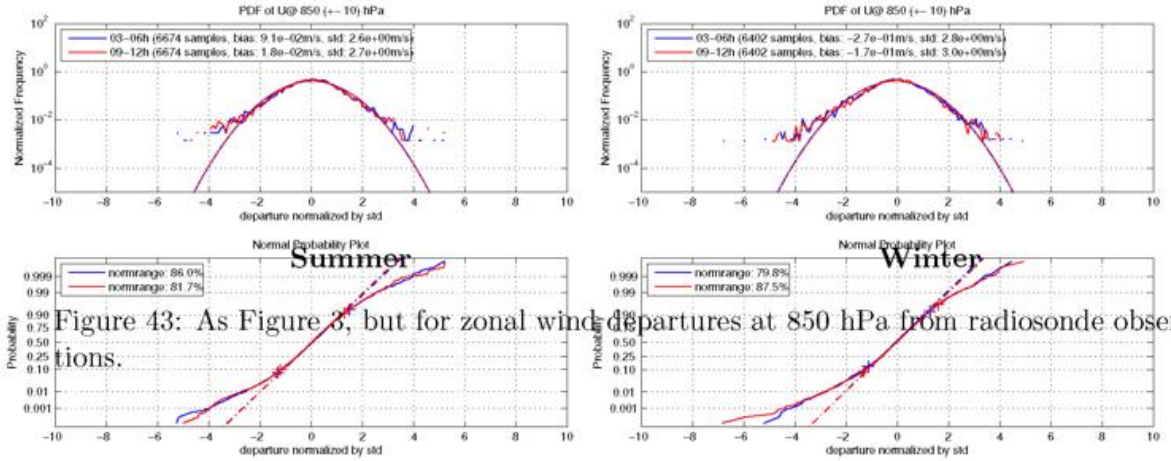

Figure 43: As Figure 3, but for zonal wind departures at 850 hPa from radiosonde observations.

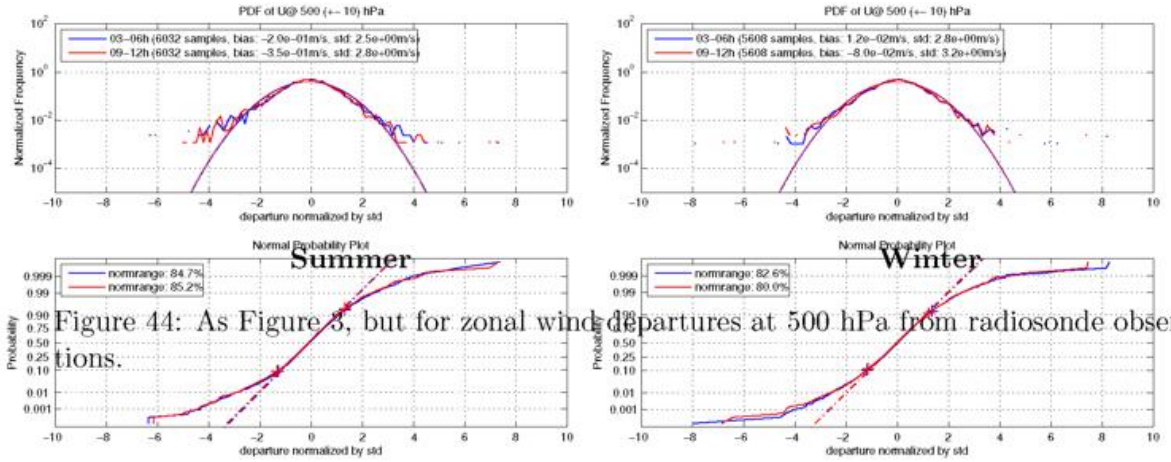

Figure 44: As Figure 3, but for zonal wind departures at 500 hPa from radiosonde observations.

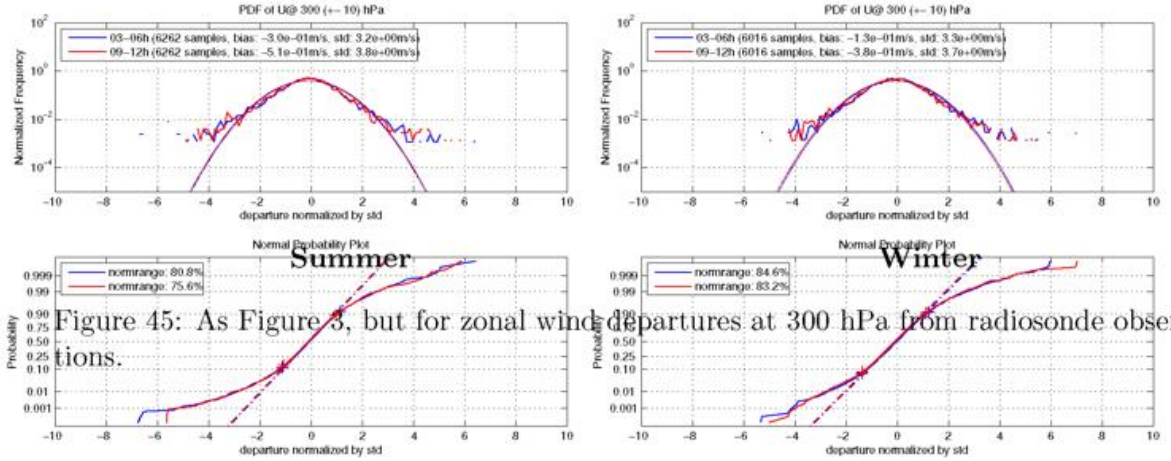

Figure 45: As Figure 3, but for zonal wind departures at 300 hPa from radiosonde observations.

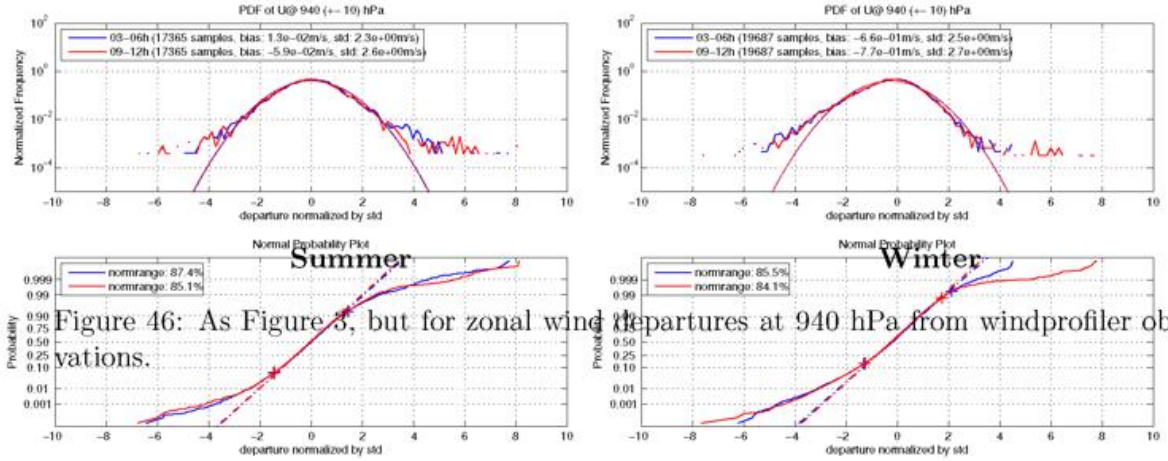

Figure 46: As Figure 3, but for zonal wind departures at 940 hPa from windprofiler observations.

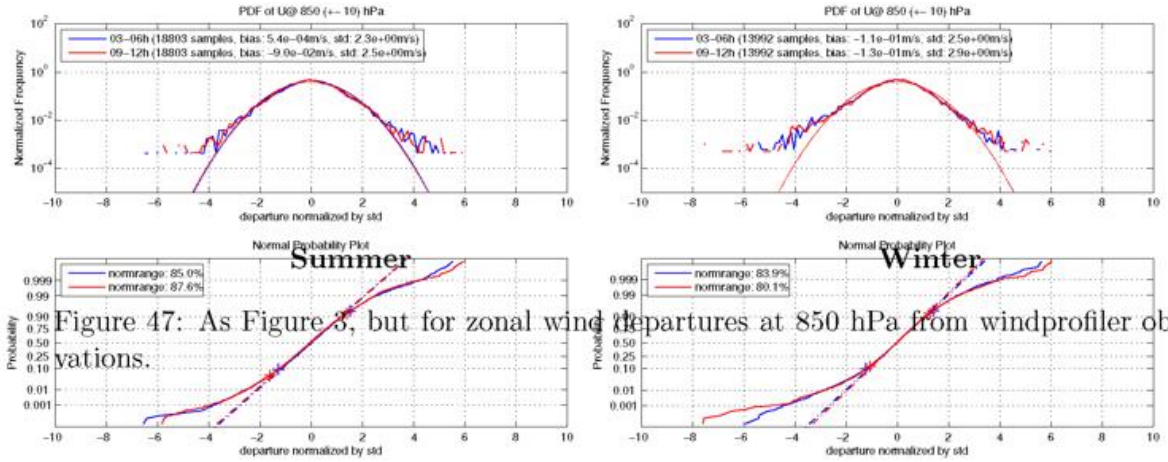

Figure 47: As Figure 3, but for zonal wind departures at 850 hPa from windprofiler observations.

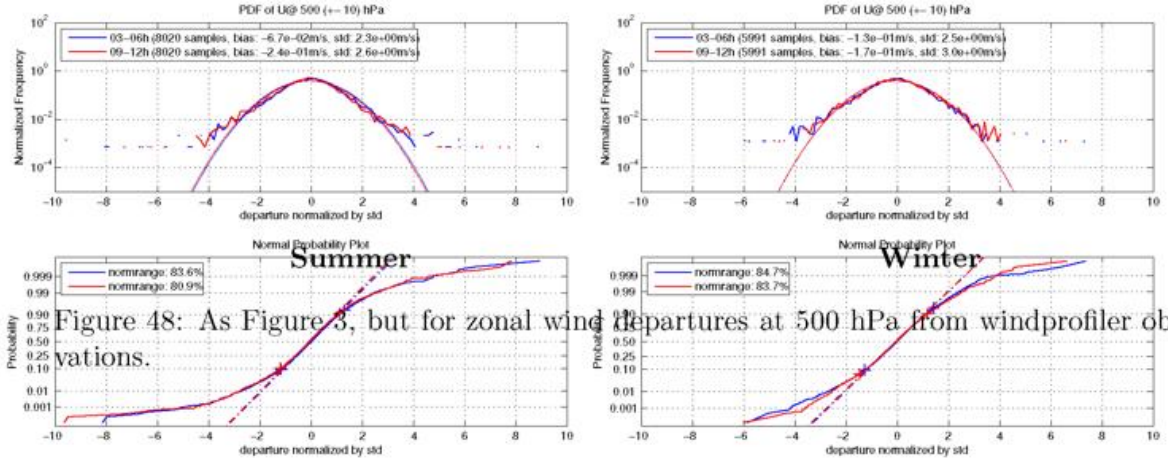

Figure 48: As Figure 3, but for zonal wind departures at 500 hPa from windprofiler observations.

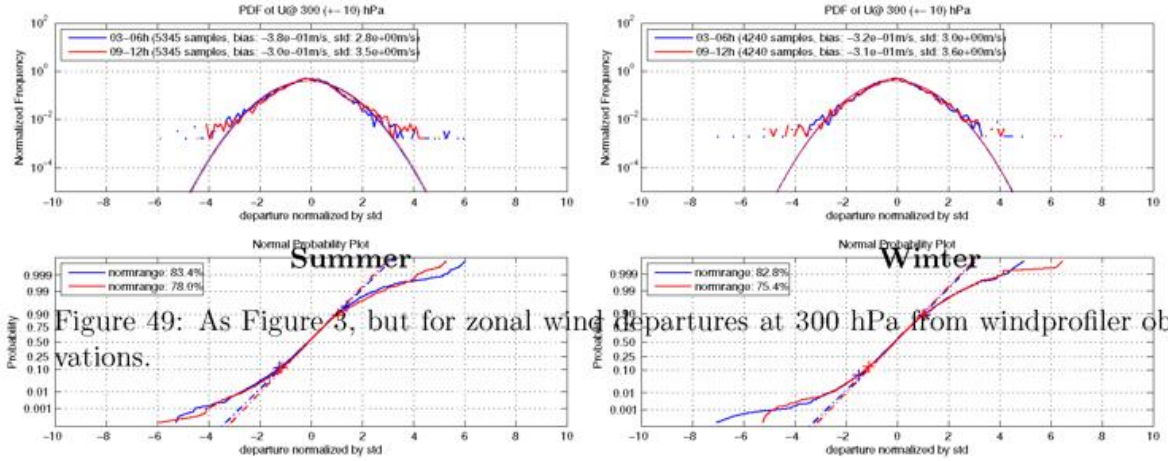

Figure 49: As Figure 3, but for zonal wind departures at 300 hPa from windprofiler observations.

5.3 Meridional wind from aircrafts, radiosondes and windprofiler

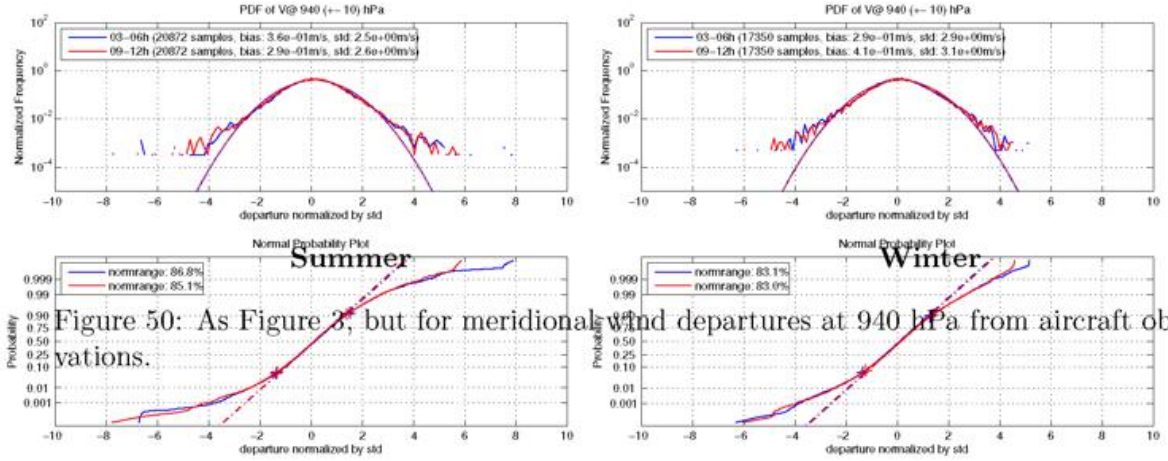

Figure 50: As Figure 3, but for meridional wind departures at 940 hPa from aircraft observations.

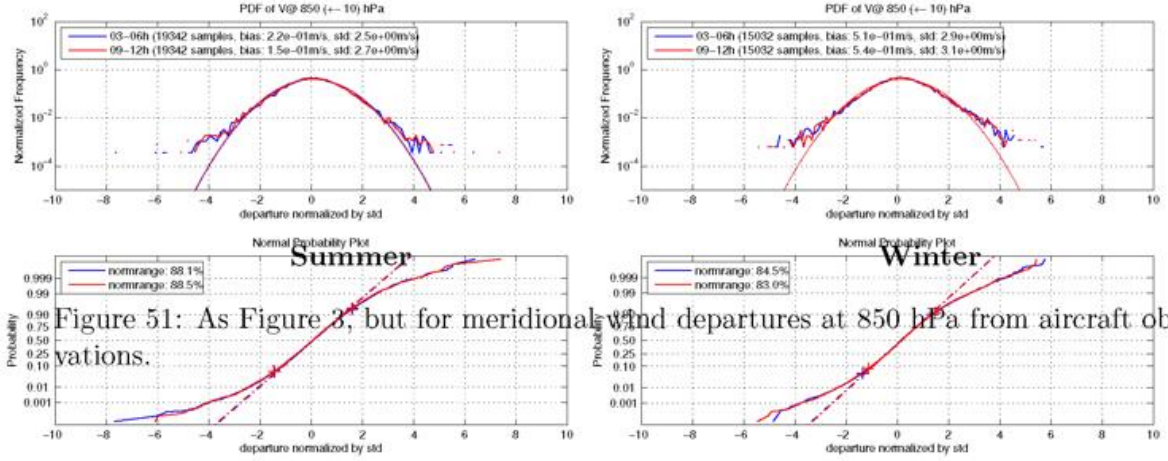

Figure 51: As Figure 3, but for meridional wind departures at 850 hPa from aircraft observations.

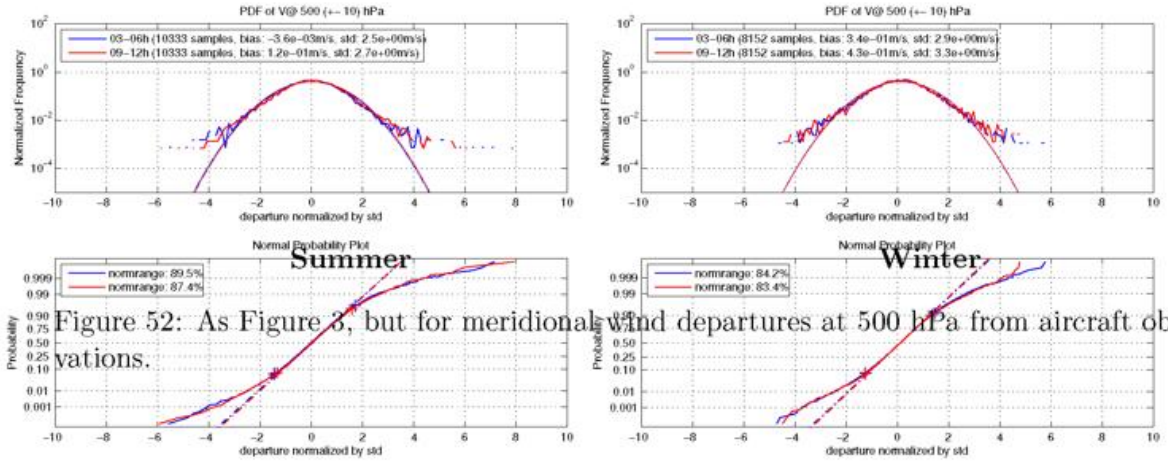

Figure 52: As Figure 3, but for meridional wind departures at 500 hPa from aircraft observations.

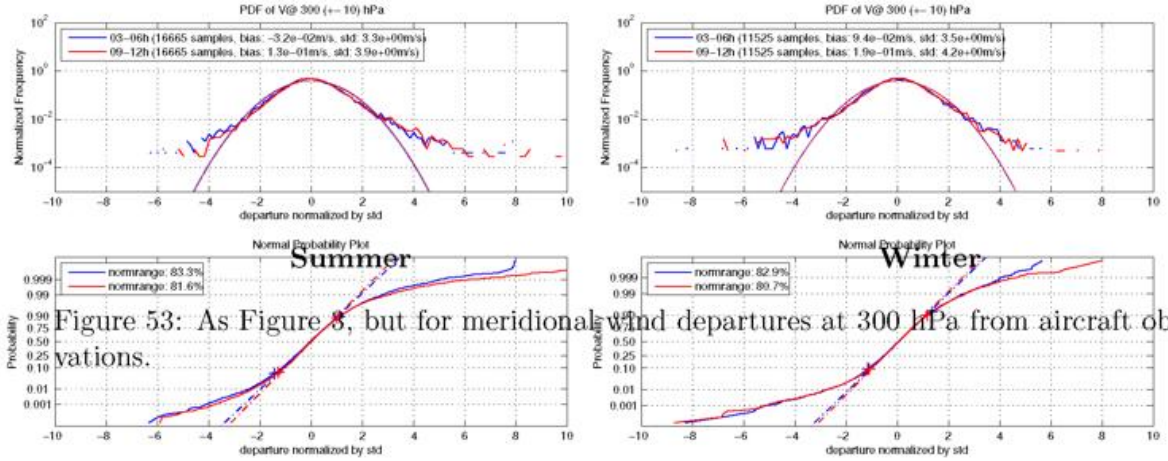

Figure 53: As Figure 3, but for meridional wind departures at 300 hPa from aircraft observations.

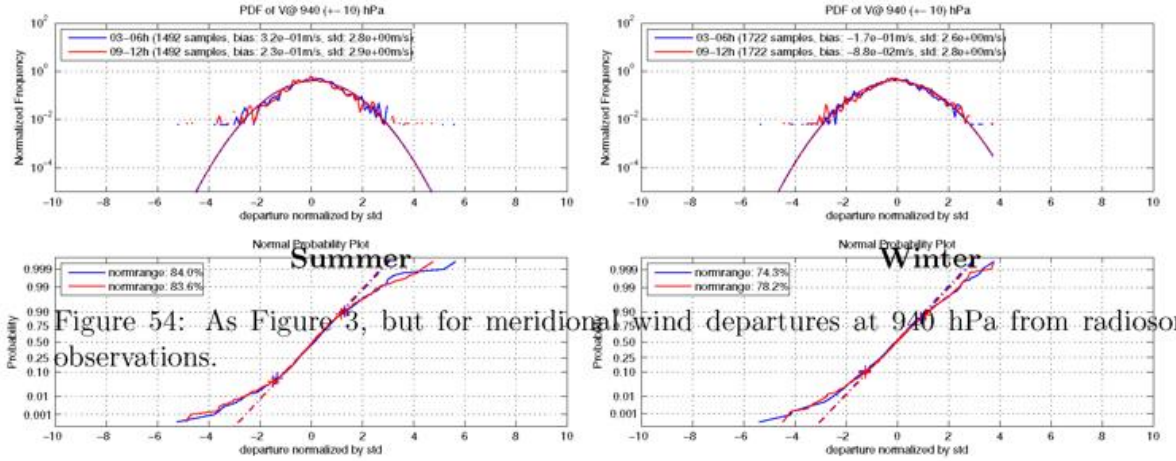

Figure 54: As Figure 3, but for meridional wind departures at 940 hPa from radiosonde observations.

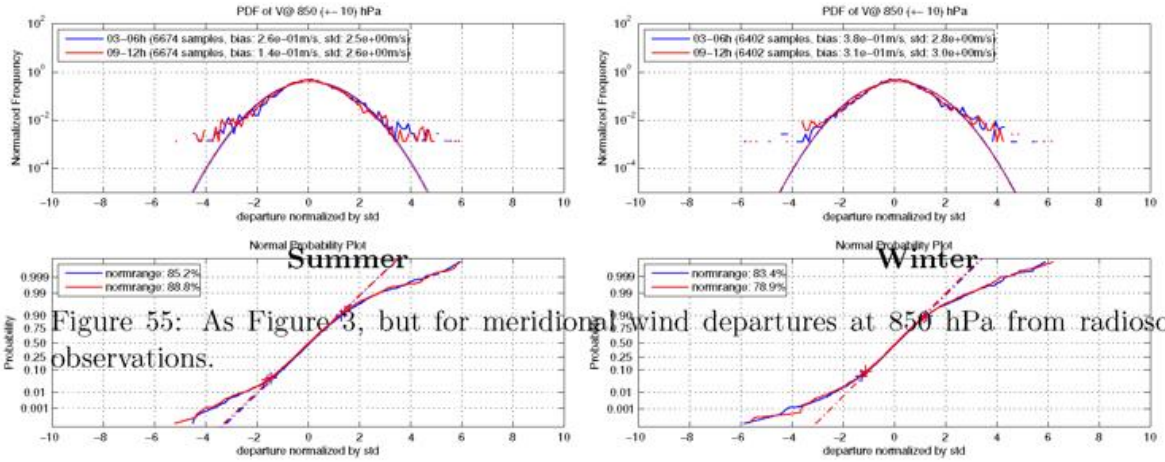

Figure 55: As Figure 3, but for meridional wind departures at 850 hPa from radiosonde observations.

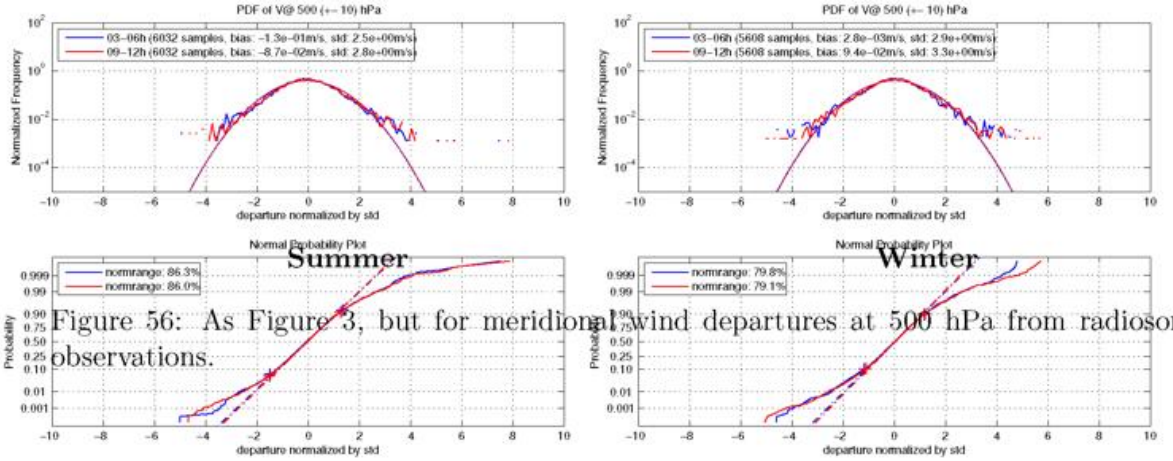

Figure 56: As Figure 3, but for meridional wind departures at 500 hPa from radiosonde observations.

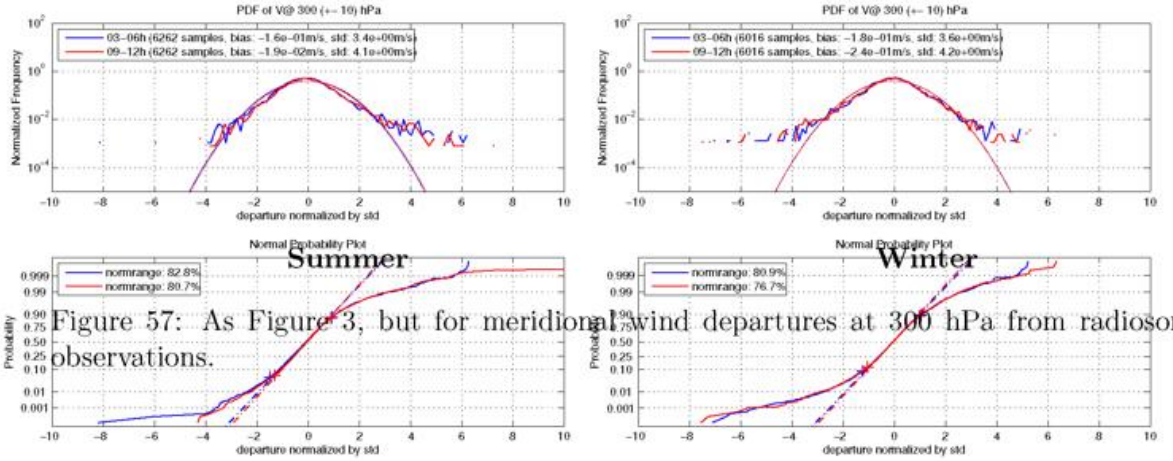

Figure 57: As Figure 3, but for meridional wind departures at 300 hPa from radiosonde observations.

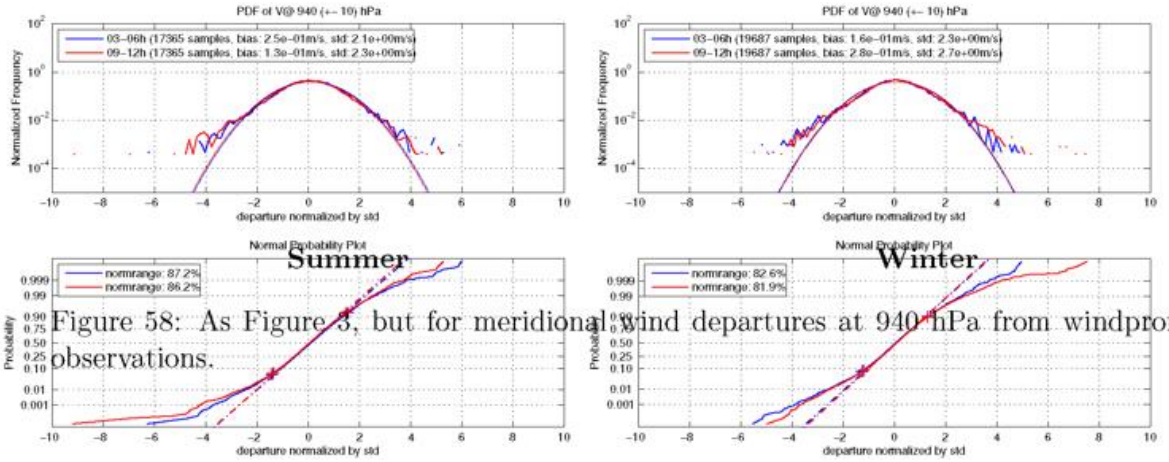

Figure 58: As Figure 3, but for meridional wind departures at 940 hPa from windprofiler observations.

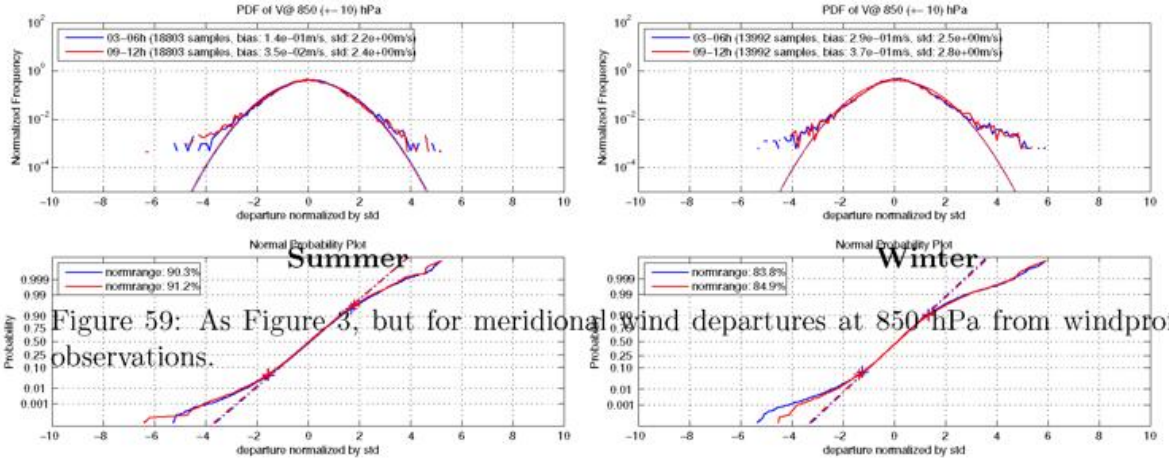

Figure 59: As Figure 3, but for meridional wind departures at 850 hPa from windprofiler observations.

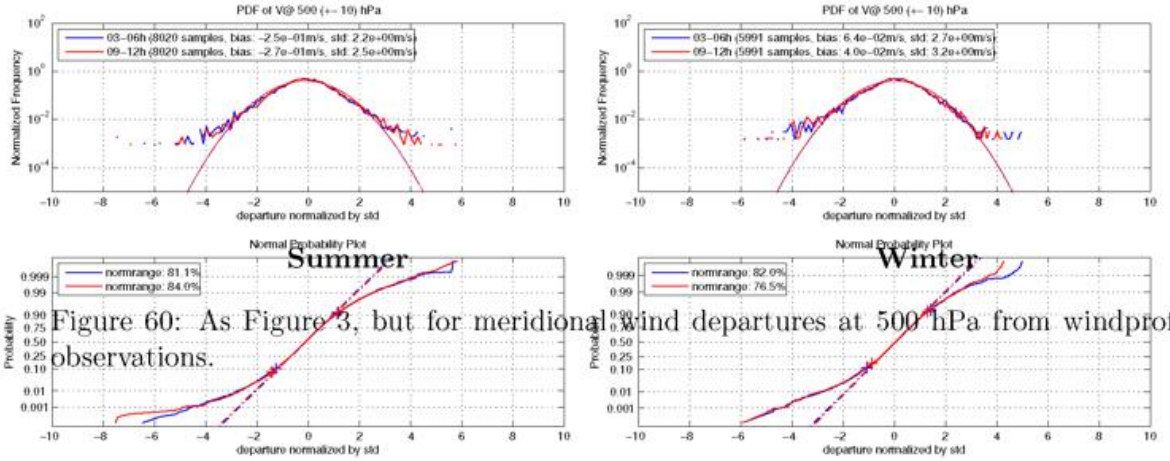

Figure 60: As Figure 3, but for meridional wind departures at 500 hPa from windprofiler observations.

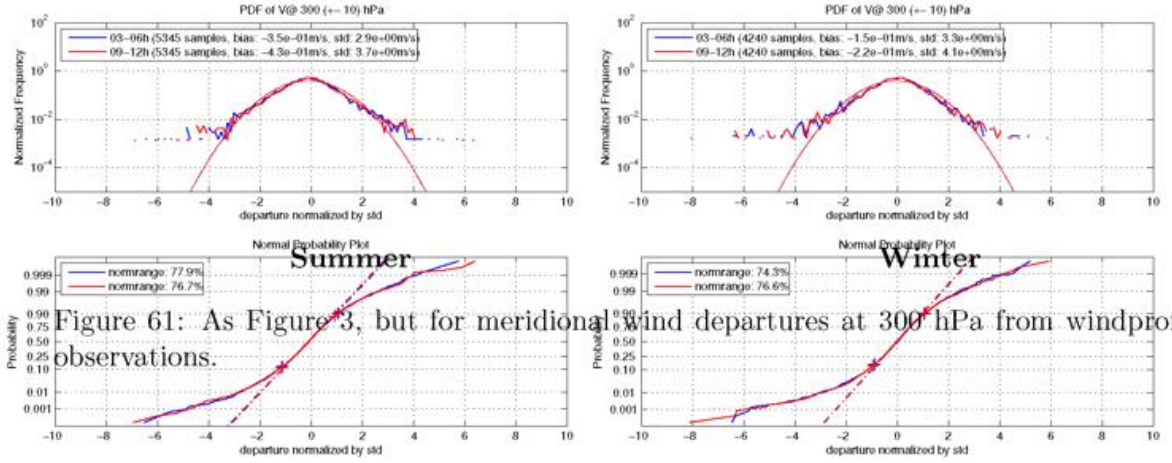

Figure 61: As Figure 3, but for meridional wind departures at 300 hPa from windprofiler observations.

6 Summary and conclusions

In this study we have investigated forecast departure distributions and ensemble background anomalies from the convection permitting COSMO model in view of the new ensemble data assimilation system for COSMO, being currently developed. Emphasis was put on how close the distributions are to the normal distribution.

Overall, the departures of most of the investigated variables show a reasonable Gaussian behaviour around the median, but exhibit more larger departures (both negative and positive) than described by a normal distribution. This behaviour (known as "fat tails") is well known in NWP data assimilation (e.g. Andersson and Järvinen, 1999; Seaman, 2008) and can be interpreted as follows: the departures belong to either of two populations, one which follows the normal Gaussian distribution, representing random errors and one which is modelled by a flat distribution, representing the population of data affected by gross errors (Andersson and Järvinen, 1999)

The main results of the study are summarized and discussed in the two following paragraphs for the forecast departures and the ensemble background anomalies, respectively.

Forecast departures

- The forecast departures of temperature, surface pressure and wind can be reasonably approximated by normal distributions. Normranges are mostly above 80%. Results among different observation systems (radiosondes, aircraft observations and windprofiler) are very similar.
- Humidity departures show a rather exponential than Gaussian distribution, relative humidity departures are more Gaussian than specific humidity departures. Normalized relative humidity departures have a much reduced bias and standard deviation and their distributions are much less dependent on the humidity itself, as compared to relative humidity.
- Surface rainfall departure distributions show a rather exponential than Gaussian shape. Departures of the logarithm of rainfall can be much better approximated by normal distributions.
- Generally, distributions are less Gaussian near the surface and in the boundary layer than in the middle and upper atmosphere.
- There is a generally slightly better Gaussian fit in summer than in winter.
- Large deviations from the Gaussian shape are found in winterly boundary layer relative humidity as a result of many near-saturated situations (stratus).
- The distributions only slightly change during the first 12 hours of forecast with the exception of surface pressure, where an increase in the bias and standard deviation is already obvious.
- The results from the convection permitting COSMO-DE model are similar to those of the regional COSMO-EU model.

One reason for the good Gaussian fit of most of the variables may be found in the fact, that the departure distributions rely on a large statistics covering all sorts of weather conditions.

A sensitivity study considering only rainy days indeed indicated that the distributions are slightly less Gaussian. However, the main findings of this study are still valid for this subsample of days.

Overall, temperature, wind and surface pressure forecast departures distributions from the convection permitting COSMO model are reasonably Gaussian out to 12 hours forecast, both in summer and winter. Humidity and rainfall are less Gaussian, but using appropriate transformations, derived humidity and rainfall variables can be found with more Gaussian distributions (e.g. normalized relative humidity and logarithm of rainfall).

Ensemble background anomalies

- At short lead times (+3h) the ensemble background anomaly distributions can deviate significantly from normality. Especially low-level temperature has been found to have multiple modes.
- Precipitation shows the similar exponential distribution as the forecast departures.
- At longer lead times (+24h) the anomaly distributions are close to normality for both, temperature and wind.
- Upper-level variables are more Gaussian than their low-level counterparts.
- The shape of the distributions are dependent on the domain under consideration. Distributions over flat terrain have been found to be closer to normality than those over more complex terrain.

The large deviations from normality at short lead times are largely due to the way the current COSMO-DE-EPS is designed. Starting from identical initial conditions (zero anomalies at the start of the forecast) the growth of the anomalies with time is first dominated by the physical parametrisation perturbations, at later times the different boundary conditions and the internal model errors start to dominate the anomaly growth. Some of the model switches systematically influence certain ensemble members, leading to a non-normal anomaly distribution at short lead times in some variables and some regions of the model domain. Therefore, in the light of an ensemble assimilation, care should be taken in the design of the physical model perturbations. The use of boundary conditions from different global models is judged as a suitable method to perturb the boundaries of the COSMO-DE-EPS in view of data assimilation, since at longer lead times, the anomaly distributions appear to be close to normality.

The error distributions found in this study closely resemble those found by Bonavita et al. (2010) using the LETKF in a regional NWP system. In particular, their distributions showed similar "fat tails" as those of the COSMO model. This slight deviation from Normality did not seem to strongly affect the performance of their application. However, as pointed out by the authors, their results did not reflect situations with strong non-linearities, such as convection. It remains to be proven that the LETKF also works in strongly convective situations. Recently, Yang and Kalnay (2009) and Kalnay and Yang (2009) proposed ways to deal with non-linearity and non-Gaussianity using the LETKF. Although they are computationally more expensive that the standard LETKF they proved to reduce the spin-up of the LETKF in highly non-linear applications and improve the Gaussianity of the errors.

Overall, the results of this study suggest that, ensemble data assimilation systems relying on the BLUE theory may well be feasible for the use with the high-resolution COSMO

model, given that more suitable (i.e. more random) physics parametrisation perturbations are applied.

References

Andersson, E., and H. Järvinen, 1999: Variational Quality Control,. *Quart. J. Roy. Meteor. Soc.*, **125**, 697–722.

Bonavita, M., L. Torrisi, and F. Marcucci, 2010: Ensemble Data Assimilation with the CNMCA Regional Forecasting System. *Quart. J. Roy. Meteor. Soc.*, accepted.

Holm, E., E. Andresson, A. Beljaars, P. Lopez, J.-F. Mahfouf, A. Simmons, and J.-N. Thépaut, 2002: Assimilation and Modelling of the Hydrological Cycle: ECMWF's Status and Plans. [ECMWF Technical Memorandum No. 383].

Hunt, B., E. Kostelich, and I. Szunyogh, 2007: Efficient data assimilation for spatiotemporal chaos: A local ensemble transform Kalman Filter. *Physica D*, **230**, 112–126.

Kalnay, E., and S.-C. Yang, 2009: Accelerating the spin-up of Ensemble Kalman Filtering. *Quart. J. Roy. Meteor. Soc.*, submitted.

Lawson, W., and J. Hansen, 2004: Implicatios of stochastic and deterministic filters as ensemble-based data assimilation methods in varying regimes of error growth. *Mon. Wea. Rev.*, **132**, 1966–1981.

Leeuwenburgh, O., G. Evensen, and L. Bertino, 2005: The impact of ensemble filter definition on the assimilation of temperature profiles in the tropical Pacific. *Quart. J. Roy. Meteor. Soc.*, **131**, 3291–3300.

Mitchell, H., and P. Houtekamer, 2009: Ensemble Kalman filter configurations and performance with the logistic map. *Mon. Wea. Rev.*, accepted.

Sakov, P., and P. Oke, 2008: Implications of the form of the ensemble transformation in the ensemble square root filter. *Mon. Wea. Rev.*, **136**, 1042–1053.

Seaman, R., 2008: The probability distribution of obeserved minus expected sea-level pressure; a quality control perspective. *Aust. Met. Mag.*, **57**, 37–43.

Yang, S.-C., and E. Kalnay, 2009: Handling Nonlinearity and Non-Gaussianity in Ensemble Kalman Filter, submitted.

List of COSMO Newsletters and Technical Reports

(available for download from the COSMO Website: www.cosmo-model.org)

COSMO Newsletters

No. 1: February 2001.

No. 2: February 2002.

No. 3: February 2003.

No. 4: February 2004.

No. 5: April 2005.

No. 6: July 2006.

No. 7: April 2008; Proceedings from the 8th COSMO General Meeting in Bucharest, 2006.

No. 8: September 2008; Proceedings from the 9th COSMO General Meeting in Athens, 2007.

No. 9: December 2008

No. 10: March 2010.

COSMO Technical Reports

No. 1: Dmitrii Mironov and Matthias Raschendorfer (2001):
Evaluation of Empirical Parameters of the New LM Surface-Layer Parameterization Scheme. Results from Numerical Experiments Including the Soil Moisture Analysis.

No. 2: Reinhold Schrodin and Erdmann Heise (2001):
The Multi-Layer Version of the DWD Soil Model TERRA_LM.

No. 3: Günther Doms (2001):
A Scheme for Monotonic Numerical Diffusion in the LM.

No. 4: Hans-Joachim Herzog, Ursula Schubert, Gerd Vogel, Adelheid Fiedler and Roswitha Kirchner (2002):
LLM ¯ the High-Resolving Nonhydrostatic Simulation Model in the DWD-Project LITFASS.
Part I: Modelling Technique and Simulation Method.

No. 5: Jean-Marie Bettems (2002):
EUCOS Impact Study Using the Limited-Area Non-Hydrostatic NWP Model in Operational Use at MeteoSwiss.

No. 6: Heinz-Werner Bitzer and Jürgen Steppeler (2004):
Documentation of the Z-Coordinate Dynamical Core of LM.

No. 7: Hans-Joachim Herzog, Almut Gassmann (2005):
Lorenz- and Charney-Phillips vertical grid experimentation using a compressible nonhydrostatic toy-model relevant to the fast-mode part of the 'Lokal-Modell'.

No. 8: Chiara Marsigli, Andrea Montani, Tiziana Paccagnella, Davide Sacchetti, André Walser, Marco Arpagaus, Thomas Schumann (2005):
Evaluation of the Performance of the COSMO-LEPS System.

No. 9: Erdmann Heise, Bodo Ritter, Reinhold Schrodin (2006):
Operational Implementation of the Multilayer Soil Model.

No. 10: M.D. Tsyrulnikov (2007):
Is the particle filtering approach appropriate for meso-scale data assimilation ?

No. 11: Dmitrii V. Mironov (2008):
Parameterization of Lakes in Numerical Weather Prediction. Description of a Lake Model.

No. 12: Adriano Raspanti (2009):
COSMO Priority Project "VERification System Unified Survey" (VERSUS): Final Report.

No. 13: Chiara Marsigli (2009):
COSMO Priority Project "Short Range Ensemble Prediction System" (SREPS): Final Report.

No. 14: Michael Baldauf (2009):
COSMO Priority Project "Further Developments of the Runge-Kutta Time Integration Scheme" (RK): Final Report.

No. 15: Silke Dierer (2009):
COSMO Priority Project "Tackle deficiencies in quantitative precipitation forecast" (QPF): Final Report.

No. 16: Pierre Eckert (2009):
COSMO Priority Project "INTERP": Final Report.

No. 17: D. Leuenberger, M. Stoll and A. Roches (2010):
Description of some convective indices implemented in the COSMO model.

No. 18: Daniel Leuenberger (2010):
Statistical analysis of high-resolution COSMO Ensemble forecasts in view of Data Assimilation.

COSMO Technical Reports

Issues of the COSMO Technical Reports series are published by the *COnsortium for Small-scale MOdelling* at non-regular intervals. COSMO is a European group for numerical weather prediction with participating meteorological services from Germany (DWD, AWGeophys), Greece (HNMS), Italy (USAM, ARPA-SIMC, ARPA Piemonte), Switzerland (MeteoSwiss), Poland (IMGW) and Romania (NMA). The general goal is to develop, improve and maintain a non-hydrostatic limited area modelling system to be used for both operational and research applications by the members of COSMO. This system is initially based on the COSMO-Model (previously known as LM) of DWD with its corresponding data assimilation system.

The Technical Reports are intended

- for scientific contributions and a documentation of research activities,
- to present and discuss results obtained from the model system,
- to present and discuss verification results and interpretation methods,
- for a documentation of technical changes to the model system,
- to give an overview of new components of the model system.

The purpose of these reports is to communicate results, changes and progress related to the LM model system relatively fast within the COSMO consortium, and also to inform other NWP groups on our current research activities. In this way the discussion on a specific topic can be stimulated at an early stage. In order to publish a report very soon after the completion of the manuscript, we have decided to omit a thorough reviewing procedure and only a rough check is done by the editors and a third reviewer. We apologize for typographical and other errors or inconsistencies which may still be present.

At present, the Technical Reports are available for download from the COSMO web site (www.cosmo-model.org). If required, the member meteorological centres can produce hard-copies by their own for distribution within their service. All members of the consortium will be informed about new issues by email.

For any comments and questions, please contact the editors:

Massimo Milelli
Massimo.Milelli@arpa.piemonte.it

Ulrich Schättler
Ulrich.Schaettler@dwd.de